A Novel Rapid Host Cell Entry Pathway Determines Intracellular Fate of *Staphylococcus aureus*

Marcel Rühling[1], Fabio Schmelz[1], Kim Ulbrich[1], Julia Wolf [1], Maximilian Pfefferle[1], Adriana Moldovan[1], Nadine Knoch[1], Andreas Iwanowitsch[1], Christian Kappe[2], Kerstin Paprotka[2], Christoph Arenz[2], and Martin J. Fraunholz[1+]

[1] Chair of Microbiology, Julius-Maximilians-University Würzburg, Theodor-Boveri-Weg, 97074 Würzburg, Germany

[2]Institut for Chemistry, Humboldt Universität zu Berlin, Brook-Taylor-Str. 2, 12489 Berlin, Germany

[+]Corresponding author: martin.fraunholz@uni-wuerzburg.de

Abstract:

Staphylococcus aureus is an opportunistic pathogen causing severe diseases. Recently, *S. aureus* was recognized as intracellular pathogen with the intracellular niche promoting immune evasion and antibiotic resistance. We identified an alternative mechanism governing cellular uptake of *S. aureus* which relies on lysosomal Ca^{2+}, lysosomal exocytosis and occurs concurrently to other well-known entry pathways within the same host cell population. This internalization pathway is rapid and active within only few minutes after bacterial contact with host cells. Compared to slow bacterial internalization, the rapid pathway demonstrates altered phagosomal maturation as well as translocation of the pathogen to the host cytosol and ultimately results in different rates of intracellular bacterial replication and host cell death. We show that these alternative infection outcomes are caused by the mode of bacterial uptake.

Introduction

The most abundant sphingolipid, sphingomyelin (SM), resides in the extracellular leaflet of the plasma membrane and hence is exposed to the environment (1, 2). SM is a substrate for sphingomyelinases (SMases) that cleave off the phosphocholine head group to produce the non-polar ceramide. Acid sphingomyelinase (ASM) is a lysosomal enzyme involved in recycling of SM (3, 4) and is linked to infectious diseases, where it was shown to be involved in cellular uptake of several human pathogens (5-11).

Staphylococcus aureus is a Gram-positive human commensal that asymptomatically colonizes about one third of the human population (12). It is an opportunistic pathogen causing diseases ranging from soft tissue and skin infections (13) to lethal diseases (14, 15). *S. aureus* is notorious for acquiring antibiotic resistances thereby causing >100,000 annual deaths (16). *S. aureus* possesses intracellular virulence strategies (17, 18) that contribute to antibiotic resistance (19, 20) and immune evasion (21).

Internalization of *S. aureus* by host cells is mediated by several adhesins on the staphylococcal surface that bind a plethora of receptors on the host cell plasma membrane (5, 22-32). For instance, staphylococcal fibronectin-binding proteins that form fibronectin bridges to $\alpha_5\beta_1$ integrins on host cells to initiate internalization (22) or clumping factor B which can interact with the host receptor annexin A2 (25).

After internalization, *S. aureus* resides within a phagosome-like compartment that matures by acquiring proteins associated with early and then late endosomes as well as lysosomes (33-35). In epithelial and endothelial cells, the bacteria translocate to the host cytosol ("phagosomal escape") where they replicate and cause host cell death (33, 36-38).

The mechanism by which pathogens enter their host cells has been suggested to dictate the outcome of infections (39-42). For instance, phagosomes formed during natural internalization of *Brucella arbortus* by macrophages possessed different characteristics compared to phagosomes that were artificially generated by phorbol myristate acetate (42). The protozoic parasite *Toxoplasma gondii* invades its host cells by a proactive mechanism. Phagosomes generated during active invasion differed from those that were generated during Fc receptor-mediated uptake of antibody-coated parasites (41). Since previous observation connecting host cell entry and intracellular fate of pathogens were based on artificial induction of internalization, it is unclear whether pathogens can enter host cells within the same population via different naturally occurring mechanisms and if the entry route has a direct influence on the outcome of an intracellular infection.

Here, we describe the internalization of *S. aureus* by tissue cells via a rapid pathway taking place within minutes after contact between bacteria and host cell surface. This pathway requires nicotinic acid adenosine dinucleotide phosphate (NAADP)-dependent mobilization of lysosomal Ca^{2+}, followed by lysosomal exocytosis and thereby release of ASM. Since the rapid uptake is concurrent to previously known internalization pathways, it probably has been missed due to long infection times used in traditional infection protocols (e.g., (22, 25, 29, 30)).

S. aureus bacteria, which enter host cells of the same cell population via the rapid pathway, cause a distinct infection outcome with altered phagosome maturation, bacterial translocation to host cytosol and eventually host cell death when compared to bacteria that enter host cells at later time points during infection. Thus, the outcome of an infection is decided at the single cell level during bacterial uptake at the host plasma membrane. Bacteria-containing phagosomes that were formed by the ASM-dependent rapid uptake pathway are delayed in their maturation and the bacteria do not escape these organelles efficiently, hence demonstrating a direct link between concurrently active modes of bacterial uptake and the resulting outcomes of intracellular *S. aureus* infection.

Results

S. aureus triggers lysosomal Ca^{2+} mobilization for host cell invasion

We previously identified that internalization of *S. aureus* by host cells is associated with cellular Ca^{2+} signaling (43). To delineate the role of Ca^{2+} in this process mechanistically, we pretreated human microvascular endothelial cells (HuLEC) with the calcium ionophore ionomycin, which reduced bacterial invasion efficiency dose-dependently (**Figure 1**, A), at concentrations neither affecting bacterial (**Supp. Figure 1**, A, B) nor host cell viability (**Supp. Figure 1**, C).

Since focal adhesions constitute major cellular entry sites for *S. aureus* and the Ca^{2+}-activated transient receptor potential ion channel 4 (TRPM4) is located therein, we inhibited TRPM4 with 9-Phenantrol. 9-Phenantrol reduced invasion efficiency (**Figure 1**, B), but was not bactericidal (**Supp. Figure 1**, D). Further, treatment of HuLEC (**Figure 1**, C) or HeLa (**Supp. Figure 1**, E) with the Ca^{2+} chelator BAPTA-AM (44) led to reduction of *S. aureus* invasion in a concentration-dependent manner.

The pore-forming staphylococcal α-toxin has been shown to mediate Ca^{2+} influx into host cells (45). However, *S. aureus* invasion was independent of toxin production in HeLa and only slightly reduced in endothelial cells (**Supp. Figure 1**, F). Consequently, omission of Ca^{2+} from the cell culture medium did not affect internalization of bacteria, indicating that invasion is not dependent on Ca^{2+} influx (**Figure 1**, C).

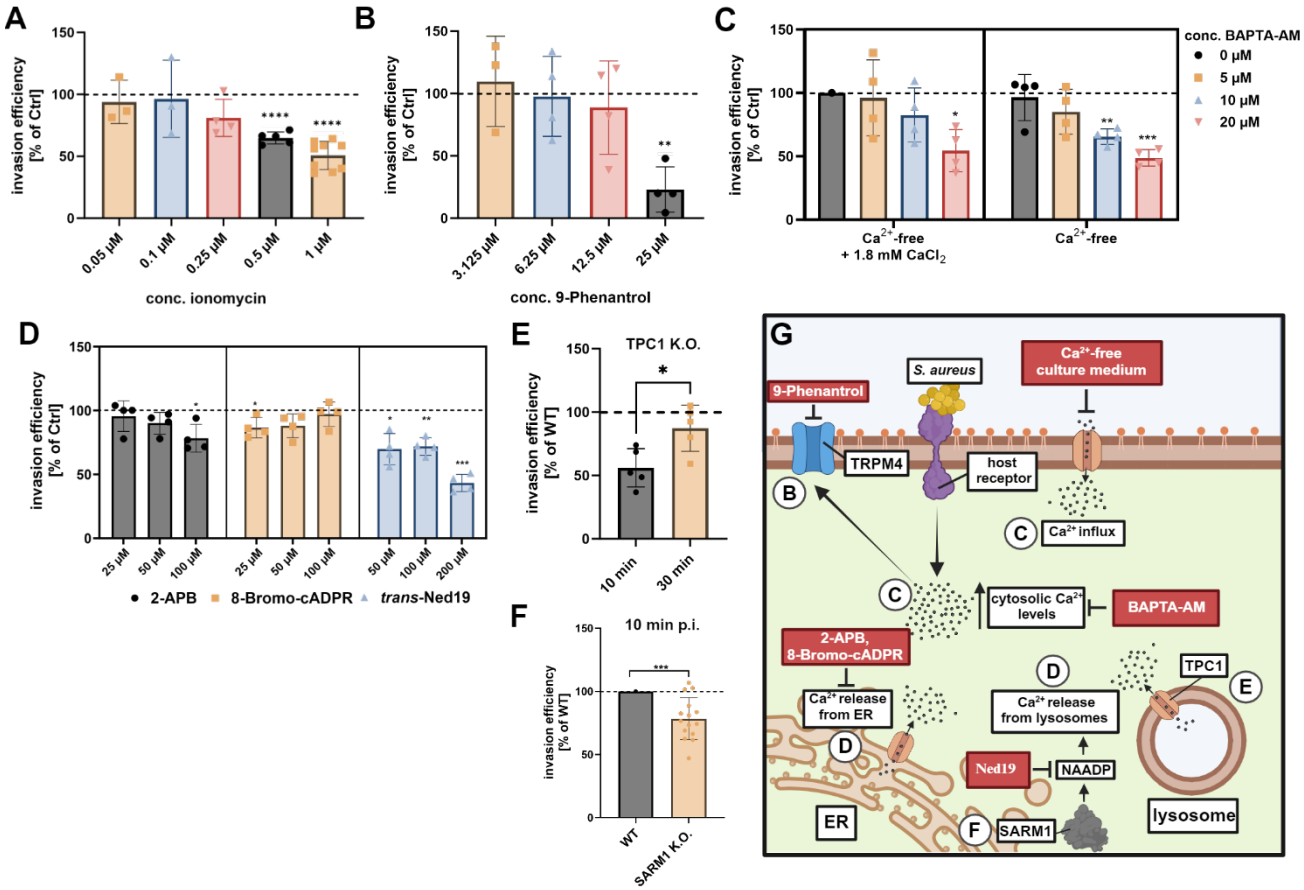

Figure 1 *S. aureus* invasion is dependent on Ca^{2+} liberation from lysosomal stores and lysosomal exocytosis. Treatment with Ionomycin (A, n≥3), 9-Phenantrol (B, n≥3), BAPTA-AM (C, n≥4), *trans*-Ned19 (D, n≥4), but not 2-APB and 8-Bromo-cADPR (D, n≥4) reduce *S. aureus* internalization by host cells in a TPC1 dependent fashion (E, n≥5). HuLEC (A, C, D, F), HeLa WT (B), HeLa TPC1 K.O. (E) or HeLa SARM1 K.O. (F) cells were treated with the respective substance and were subsequently infected with *S. aureus* JE2 for 30 min if not indicated otherwise. Extracellular bacteria were removed by lysostaphin, and the number of intracellular bacteria was determined by CFU counting. Results were normalized to untreated controls to obtain invasion efficiency (in

percent of control). (F) scheme of host cell Ca^{2+} signaling and interfering agents. Statistics: one sample t-test (A-D, F), unpaired Student´s t-test (E). Bars represent means ± SD. *p≤0.05, **p≤0.01, ***p≤0.001, ****p≤0.0001.

Since intracellular Ca^{2+} stores can serve as alternative source of Ca^{2+}, we next blocked Ca^{2+} liberation from the ER using 2-APB (46) or 8-Bromo-cyclic ADP ribose (8-Bromo-cADPR; (47)) and from lysosomes using *trans*-Ned19 (48) in HuLEC (**Figure 1***,* D) or HeLa (**Supp. Figure 1***,* G, H) at concentrations not affecting bacterial viability (**Supp. Figure 1**, I and J). Interference with lysosomal, but not ER Ca^{2+} release reduced internalization of *S. aureus*.
Ned19 antagonizes NAADP, a second messenger that mediates opening of two pore channels (TPCs) which transport Ca^{2+} from the endo-lysosomal compartment into the cytosol (48). Hence, a HeLa cell pool depleted of TPC1 (**Supp. Figure 1***,* K) substantially reduced invasion when compared to unmodified HeLa cells. This was particularly pronounced after a 10 min infection pulse, suggesting that Ca^{2+}-dependent invasion is important early in infection (**Figure 1**, E).
CD38 is a well-known producer of NAADP in immune cells (49-51). Thus, we tested *S. aureus* invasion in HeLa cells treated with the specific CD38 inhibitor 78c, even though expression of CD38 in these cells is predicted to be very low (proteinatlas.org). We observed no effect on *S. aureus* invasion by CD38 inhibition (**Supp. Figure 1**, L). An alternative NAADP producer, with higher expression in our infection model, is *Sterile Alpha and TIR Motif Containing 1* [SARM1, (52)]. We measured a slightly decreased invasion efficiency 10 min p.i. in a cell pool lacking SARM1 when compared to WT cells (**Figure 1**, F; **Supp. Figure 1**, M), suggesting that SARM1 might be enrolled in NAADP production during internalization of *S. aureus* by host cells.
Altogether, our findings support the important role of lysosomal Ca^{2+} mobilization in *S. aureus* invasion as particularly required early in infection.

Rapid S. aureus invasion requires lysosomal exocytosis, ASM and its substrate sphingomyelin on the host cell surface

Ionomycin treatment results in lysosomal exocytosis, a Ca^{2+}-dependent process in which lysosomes release their content to the extracellular space (45, 53). Hence, we treated host cells with Vacuolin-1, an inhibitor blocking this process (54), which reduced invasion efficiency in HuLEC (**Figure 2**, A) and HeLa cells (**Supp. Figure 2***,* A), while not affecting survival of the bacteria (**Supp. Figure 2***,* B).
Synaptotagmin 7 (Syt7) is known to support fusion of lysosomes with the plasma membrane in a Ca^{2+}-dependent manner (55). Accordingly, Syt7-depleted HeLa cells demonstrated lower bacterial invasion (**Figure 2**, B). As already observed for TPC1 (**Figure 1**, E), this was most pronounced early in infection further supporting our hypothesis that lysosomal exocytosis is important for rapid invasion events.
Lysosomal exocytosis results in release of ASM (45, 56). Therefore, prior to infection, the cells were exposed to amitriptyline, a functional inhibitor of ASM (FIASMA), or a competitive inhibitor [ARC39, (57)] at concentrations not affecting bacterial survival (**Supp. Figure 2**, C, D). While invasion in HuLEC, human umbilical vein endothelial cells (HuVEC) and HeLa was sensitive to both inhibitors, invasion in 16HBE14o^{-} and EA.hy926 was not or only marginally affected (**Figure 2***,* C). We excluded that differences among cell lines arose from differential ASM activity or sensitivity to the inhibitors by monitoring enzymatic activity [**Supp. Figure 2***,* E; (58) and **Supp. Figure 2***,* F; (59)].
Next, we treated HuLEC with 10 µM ARC39 or 0.5 µM PCK310, a fast-acting ASM inhibitor. Already after 1h preincubation, PCK310 reduced invasion of *S. aureus*, whereas ARC39 required overnight treatment for a similar reduction (**Figure 2***,* D). Taken together, these results show that ASM is involved in *S. aureus* invasion of host cells.

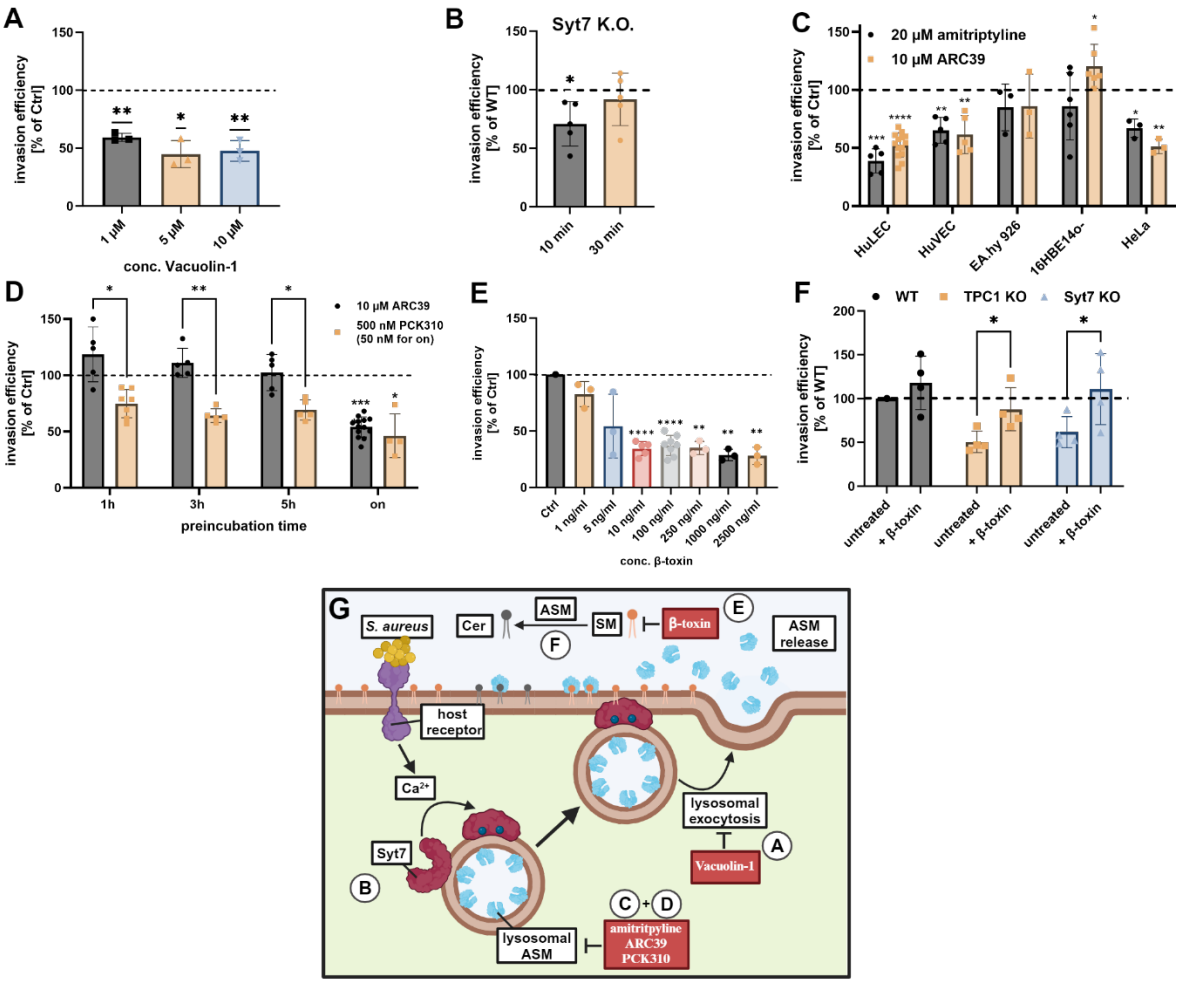

Figure 2 *S. aureus* invasion requires lysosomal exocytosis, ASM and plasma membrane sphingomyelin. **(A, B) *S. aureus* invasion requires Syt7-dependent lysosomal exocytosis.** HuLEC were treated with the lysosomal exocytosis inhibitor Vacuolin-1 and invasion efficiency of *S. aureus* was determined 30 min p.i. (A, n=3). Invasion efficiency of *S. aureus* JE2 was determined in HeLa Syt7 K.O. cells 10 min and 30 min p.i. (B, n=5; data normalized to HeLa WT). **(C, D) *S. aureus* internalization is dependent on ASM activity in endothelial and epithelial cells.** Indicated cell lines were treated with the ASM inhibitors amitriptyline or ARC39 (C) and invasion efficiency of *S. aureus* was determined (n≥3). (D) HuLEC were treated with PCK310 or ARC39 for the indicated periods. Subsequently, cells were infected with *S. aureus* for 30 min and invasion efficiency was determined by CFU counting (n≥4). **(E, F) *S. aureus* invasion requires SM and SMase activity on host cell plasma membranes.** HuLEC were treated with the bacterial SMase β-toxin for 75 min and were subsequently infected with *S. aureus* JE2 for 30 min (n≥3). **(F) Presence of extracellular SMase activity restores invasion defect in TPC1 and Syt7 K.O. cell lines.** HeLa wild type as well as TPC1 or Syt7 KO cell lines were infected with *S. aureus* JE2 in presence of 100 ng/ml of the bacterial SMase β-toxin and invasion efficiency 10 min p.i. was determined (n=4). In each experiment the numbers of intracellular *S. aureus* JE2 were determined by lysostaphin protection assay and CFU counting. Results obtained for the tested condition were normalized to the wildtype cell line or the mock-treated control. **(G) scheme of lysosomal exocytosis and ASM release as well as interfering agents.** Cer: ceramide, SM: sphingomyelin, ASM: acid sphingomyelinase. Statistics: one sample t-test (A-C, E), one-way ANOVA and Dunnett's multiple comparisons test (D). Two-way ANOVA and Tukey's multiple comparison (F). Bars represent means ± SD. *p≤0.05, **p≤0.01, ***p≤0.001, ****p≤0.0001.

We removed SM, the substrate of ASM, from plasma membranes of HuLEC (**Figure 2**, E) and HeLa (**Supp. Figure 2**, G) by pretreatment with the bacterial SMase β-toxin. Most human pathogenic *S. aureus* strains including JE2, the strain we use in the present study, do not produce β-toxin, due to a genomic integration of a prophage (60). SMase pretreatment reduced invasion efficiency in a concentration-dependent manner in both cell lines. 10 ng/ml β-toxin were sufficient to decrease invasion to 34.37 ± 6.24% of that measured in untreated control cells. Interestingly, a 250-fold higher

concentration did not lead to further reduction. In line with our previous experiments, this suggests that multiple *S. aureus* invasion pathways exist within the same host cell population, of which at least one requires SM and its enzymatic breakdown on the plasma membrane.

Next, we infected wild-type as well as the TPC1 or Syt7 K.O. cells with *S. aureus* in presence (but without pretreatment) of 100 ng/ml β-toxin and determined the number of intracellular bacteria after 10 min (**Figure 2**, F). Presence of β-toxin in the culture medium completely rescued the invasion defect of the K.O. cells. This indicates that reduced bacterial internalization in absence of TPC1 and Syt7 results from a lack in ASM delivery to the cell surface by Ca^{2+}-dependent lysosomal exocytosis.

ASM- and Ca^{2+}-mediated invasion is rapid

To study the role of SM in *S. aureus* uptake kinetics, we incubated HuLEC with fluorescent sphingolipid analogs and recorded *S. aureus* infection by time lapse imaging [**Figure 3**, A; **Supp. Video 1**; **Supp. Figure 3**; **Supp. Video 2**; (59)]. We observed that the bacteria were rapidly engulfed by SM-containing membrane compartments. While association of bacteria with BODIPY-FL-C12-SM increased over time during the first 30 min of infection, this was not observed for BODIPY-FL-C12-Ceramide, suggesting that *S. aureus* invasion specifically relies on interaction with SM in plasma membranes (**Figure 3**, B).

Next, we determined the invasion efficiency of *S. aureus* in a time-dependent manner and blocked invasion by either ASM inhibitors, ionomycin, BAPTA-AM or β-toxin pretreatment. We found a time-dependent increase in intracellular bacteria, whereby all treatment conditions reduced bacterial invasion at every time point with the untreated control at 30 min set to 100% (**Figure 3**, C). By normalizing the data to the untreated control at the corresponding time points, we found that -with exception of β-toxin- the effect of the treatments was most pronounced early (5-10 min) after infection (**Figure 3**, D). Thus, early during infection bacteria enter the host cell predominantly in an ASM- and Ca^{2+}-dependent manner.

The mode of S. aureus invasion affects infection outcome

After invasion, *S. aureus* resides within Rab5-positive early and subsequently, in Rab7-positive late phagosomes (33). We pretreated a HeLa cell line stably expressing mCherry-Rab5 as well as YFP-Rab7 with amitriptyline and infected with *S. aureus* for different time periods and determined the proportion of bacteria that associated with Rab5 and/or Rab7 (**Figure 4**, A).

While ASM inhibition marginally affected *S. aureus* association with Rab5-positive phagosomes, that with the Rab7-positive compartment was significantly reduced compared to the untreated control. This was restricted to shorter infection pulses (5-45 min) and was not observed for long infection periods (60 min). We also observed a reduced proportion of bacteria associating with Rab7-positive membranes after treatment with PCK310 or bacterial SMase. However, this was not caused by translocation of *S. aureus* to the host cytosol (**Supp. Figure 4**, A, B). Hence, phagosomes generated ASM-dependently possess different maturation dynamics when compared to phagosomes formed in an ASM-independent fashion.

Next, we measured phagosomal escape while simultaneously detecting SM content of disrupted phagosomal membranes. Therefore, we used a HeLa reporter cell line that cytosolically expresses the phagosomal escape reporter RFP-CWT (36) as well as the SM reporter $Lysenin^{W20A}$-YFP (61), respectively (**Figure 4**, B). Reporter gene expression in the cell line did not alter *S. aureus* invasion dynamics under different treatment conditions (**Supp. Figure 4**, C). The reporter cells were left untreated or were pre-exposed to ASM inhibitors and were infected with *S. aureus* strain JE2. In addition, *S. aureus* Cowan I, a strain known to have low escape rates, was used for infection. The proportion of bacteria that escaped from the phagosome (**Figure 4**, C) as well as the proportion of escape events that additionally were positive for cytosolic SM (**Supp. Figure 4**, D) were determined 1.5 h and 3 h p.i. (see also **Supp. Figure 5**, A-D).

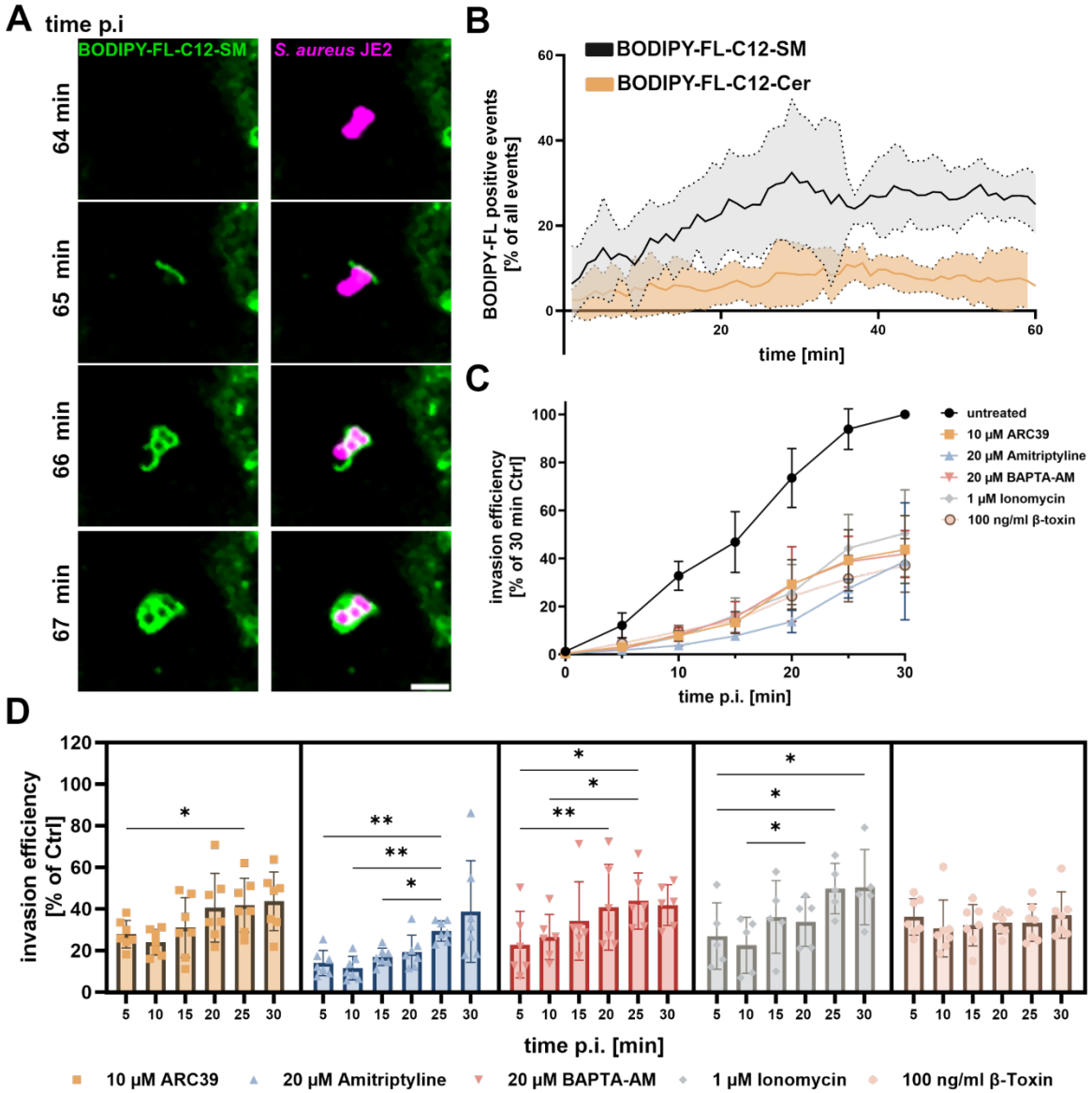

Figure 3 ASM- and Ca^{2+}-dependent uptake is rapid and predominantly mediates invasion early in infection. (A, B) *S. aureus* associates with SM early during invasion. HuLEC were pretreated with BODIPY-FL-C12-SM or BODIPY-FL-C12-ceramide and infected with red-fluorescent *S. aureus*. Scale bar: 5 µm. Infection was monitored by live cell imaging and the proportion of bacteria that associated with the lipid analogs was quantified in each individual frame (SM: n=5, Cer: n=3). **(C, D) ASM and Ca^{2+}-dependent invasion is rapid.** HuLEC were treated with ARC39, amitriptyline, BAPTA-AM, ionomycin, or the bacterial SMase β-toxin. Then, cells were infected with *S. aureus* and the number of invaded bacteria was determined after different time periods. The results were either normalized to 30 min time point of untreated controls (C) or to the corresponding time points of the untreated controls (D). (n ≥5). Statistics: Mixed effect analysis and Tukey's multiple comparison. Graphs represent means ± SD. *p≤0.05, **p≤0.01, ***p≤0.001, ****p≤0.0001.

Whereas no differences for Lysenin-positive escape events were detected (**Supp. Figure 4**, D), a higher proportion of bacteria escaped from phagosomes on abrogation of ASM activity regardless of the inhibitor used (**Figure 4**, C; **Supp. Figure 4**, E). A similar increase was observed when we blocked lysosomal exocytosis by Vacuolin-1 (**Supp. Figure 4**, F).

Since blocking of ASM-dependent uptake reduced the number of intracellular bacteria but increased their phagosomal escape rates, we hypothesized that the presence of SM on the plasma membrane affects downstream events during *S. aureus* infection. To address this question, we pretreated host cells with the bacterial SMase β-toxin to block SM-dependent invasion (**Figure 4**, D; 2a, 2b) and either infected

239 the cells in presence (3a) or after removal of the toxin (3b). β-toxin pretreatment, resulted in enhanced
240 phagosomal escape rates of *S. aureus* JE2, independent of the presence of β-toxin during infection
241 (**Figure 4**, E; 4a, 4b). This was not observed for infection with the non-cytotoxic Cowan I strain,
242 indicating that removal of SM by β-toxin did not affect general phagosomal membrane stability (**Supp.**
243 **Figure 4**, G). Moreover, β-toxin treatment strongly reduced recruitment of Lysenin^{W20A}, demonstrating
244 effective removal of SM from membranes by β-toxin (**Figure 4**, F and **Supp. Figure 5**, E-J).
245 To investigate if removal of SM was important at the cell surface or within the phagosome, we infected
246 the cells with an *S. aureus* JE2 strain recombinantly overexpressing β-toxin and Cerulean, or a strain
247 solely expressing Cerulean. We did not observe increased phagosomal escape upon overexpression of
248 β-toxin (Figure 5, E; 4c), although SM levels of phagosomal membranes were reduced (Figure 5, F)
249 comparably to samples pretreated with β-toxin (see above). Moreover, we did not detect substantial
250 differences in escape rates of *S. aureus* 6850, a strain naturally producing β-toxin (**Supp. Figure 4**, H),
251 and an isogenic β-toxin mutant. By contrast, escape of *S. aureus* 6850 again was enhanced upon
252 pretreatment with β-toxin (**Supp. Figure 4**, I) accompanied by absence of SM from phagosomal
253 membranes (**Supp. Figure 4**, J).
254 Phagosomal escape of *S. aureus* thus is independent of SM levels within the infected phagosomes, but
255 rather reflects the presence of SM and ASM at the plasma membrane during host cell entry.
256
257 To demonstrate that phagosomal escape is dependent on the pathway of cell entry, we infected reporter
258 cells with *S. aureus* for either a 10 min ("early invaders") or a 30 min infection pulse ("early and late
259 invaders"). Subsequently, we determined phagosomal escape rates (**Figure 4**, H) as well as the number
260 of invaded bacteria (**Supp. Figure 4**, K). Independent of the multiplicity of infection (MOI) used,
261 bacteria taken up within the first 10 min demonstrated significantly lower escape rates when compared
262 to bacteria that were cocultured with host cells for 30 min.
263 This was corroborated by HeLa YFP-CWT infected with *S. aureus* expressing a fluorescent protein (e.g.
264 mRFP) for 30 min ("early and late invaders"). After 20 min, we initiated a second infection pulse for 10
265 min ("early invaders") with a *S. aureus* strain expressing another fluorescence protein (e.g. Cerulean)
266 and determined phagosomal escape rates of both bacterial recombinants (**Figure 4**, I). Again, early
267 invaders demonstrated lower escape rates when compared to the 30 min control. This was independent
268 of the fluorescence expressed by the strain that was used for each infection pulse.
269

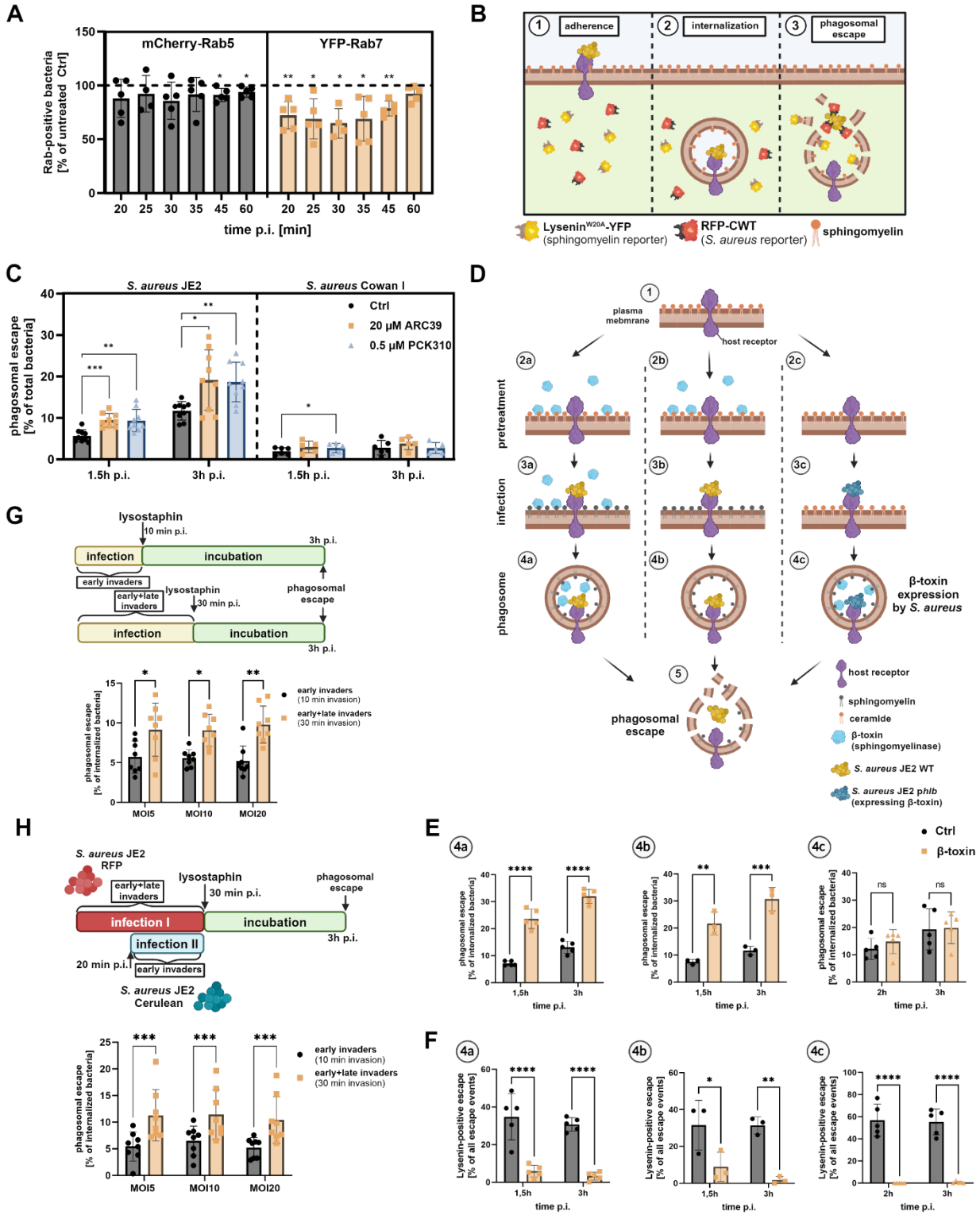

Figure 4 The intracellular fate of *S. aureus* is determined by the pathway of cell entry.
(A) Inhibition of ASM delays formation of Rab7-positive phagosomes. HeLa cells expressing mCherry-Rab5 and YFP-Rab7 were either treated with amitriptyline or left untreated. Then, cells were infected with *S. aureus* JE2 for indicated periods. Extracellular bacteria were removed and proportion of intracellular bacteria associating with Rab5 or Rab7 was determined by CLSM. Results obtained for amitriptyline-treated samples were normalized to untreated controls (n=5). **(B) Detection of phagosomal SM and phagosomal escape by a reporter cell line expressing Lysenin^{W20A} -YFP and RFP-CWT.** After internalization, *S. aureus* resides in a phagosome preventing the recruitment of RFP-CWT to *S. aureus* cell wall and Lysenin^{W20A}-YFP to luminal SM, respectively. When the bacteria lyse the phagosomal membrane, luminal SM gets exposed to the cytosol and attracts Lysenin^{W20A} -YFP, while RFP-CWT is recruited to the staphylococcal surface. **(C) Blocking ASM-dependent internalization affects**

phagosomal escape. RFP-CWT and Lysenin^{W20A} -YFP expressing HeLa were treated with PCK310, or ARC39 and infected with *S. aureus* strains JE2 or Cowan I. Thereby, β-toxin was either removed prior to infection (pretreatment only) or was present during the whole experiment (pretreatment + during infection). By CLSM, proportions of bacteria that recruited RFP-CWT (phagosomal escape) were determined (n≥3). **(D-F) Phagosomal escape depends on presence of plasma membrane SM during invasion, but not presence of SM within phagosomal membranes** HeLa RFP-CWT Lysenin^{W20A} -YFP were pretreated with β-toxin to remove surface SM (2a, 2b) or left untreated (2c). Then, cells were infected with *S. aureus* JE2 in presence (3a) or absence (3b) of β-toxin. Untreated samples (3c) were infected with *S. aureus* JE2 harboring a plasmid either encoding β-toxin and the fluorescence protein Cerulean (pCer+*hlb*) or solely Cerulean (pCer). Proportion of bacteria that recruited RFP-CWT (phagosomal escape, E) and the percentage of phagosomal escape events that additionally were positive for Lysenin^{W20A}-YFP (F) were determined at indicated time points p.i. (n=5). **(G, H) Early ASM-dependent invaders possess lower escape rates than late invaders.** HeLa cells expressing RFP-CWT were infected with indicated MOIs of *S. aureus* JE2 either for 10 min (early invaders) or 30 min (early+late invaders). Phagosomal escape rates were determined 3h p.i. (G). HeLa reporter cells expressing YFP-CWT were infected with an MOI=5 of *S. aureus* JE2 expressing a fluorescent protein (e.g. RFP) for 30 min (early+late invaders). After 20 min, the same samples were infected with *S. aureus* JE2 expressing another fluorophore (e.g. Cerulean) for 10 min (early invaders) and phagosomal escape was determined 3 h p.i. (H). **Statistics:** one sample t-test (A), Mixed effects analysis (REML) and Tukey's multiple comparison (C,G, H), Two-way ANOVA and Šídák's multiple comparisons test (E, F). Graphs represent means ± SD. *p≤0.05, **p≤0.01, ***p≤0.001, ****p≤0.0001.

We next monitored phagosomal escape over 10 h in cells pretreated with ASM inhibitors (**Figure 5**, A). The compounds enhanced escape rates 3 h p.i. when compared to untreated controls. In contrast, 6 h p.i. escape rates were found decreased upon ASM inhibition.

Taken together, the efficiency of phagosomal escape of *S. aureus* is directly affected by the mode of cell entry, whereby the rapid SM/ASM-dependent pathway results in delayed phagosomal escape, while bacteria that entered host cells ASM-independently escape earlier during infection.

Since translocation to the host cytosol is a prerequisite for *S. aureus* replication in non-professional phagocytes, we recorded intracellular growth of *S. aureus*. In untreated controls replication started about 5 h p.i., and thus shortly after phagosomal escape (3-4 h p.i., **Figure 5**, B). By contrast, we did not observe significant bacterial replication in cells treated with ASM inhibitors (**Figure 5**, B).

We next treated HuLEC with β-toxin, stained the cells with BODIPY-FL-C12-SM and infected the cells with fluorescent *S. aureus*. Live cell imaging demonstrated that most untreated host cells died after 11 h p.i., whereas β-toxin-treated samples showed higher survival rates (**Figure 5**, C). This was also observed by cell death assays measuring i) membrane integrity (7-AAD staining, **Figure 5**, D), ii) apoptosis (Annexin V staining, **Figure 5**, E), iii) number of host cells that remained attached to the substratum (**Supp. Figure 6**, A) and iv) host cell lysis by LDH release (**Supp. Figure 6**, B).

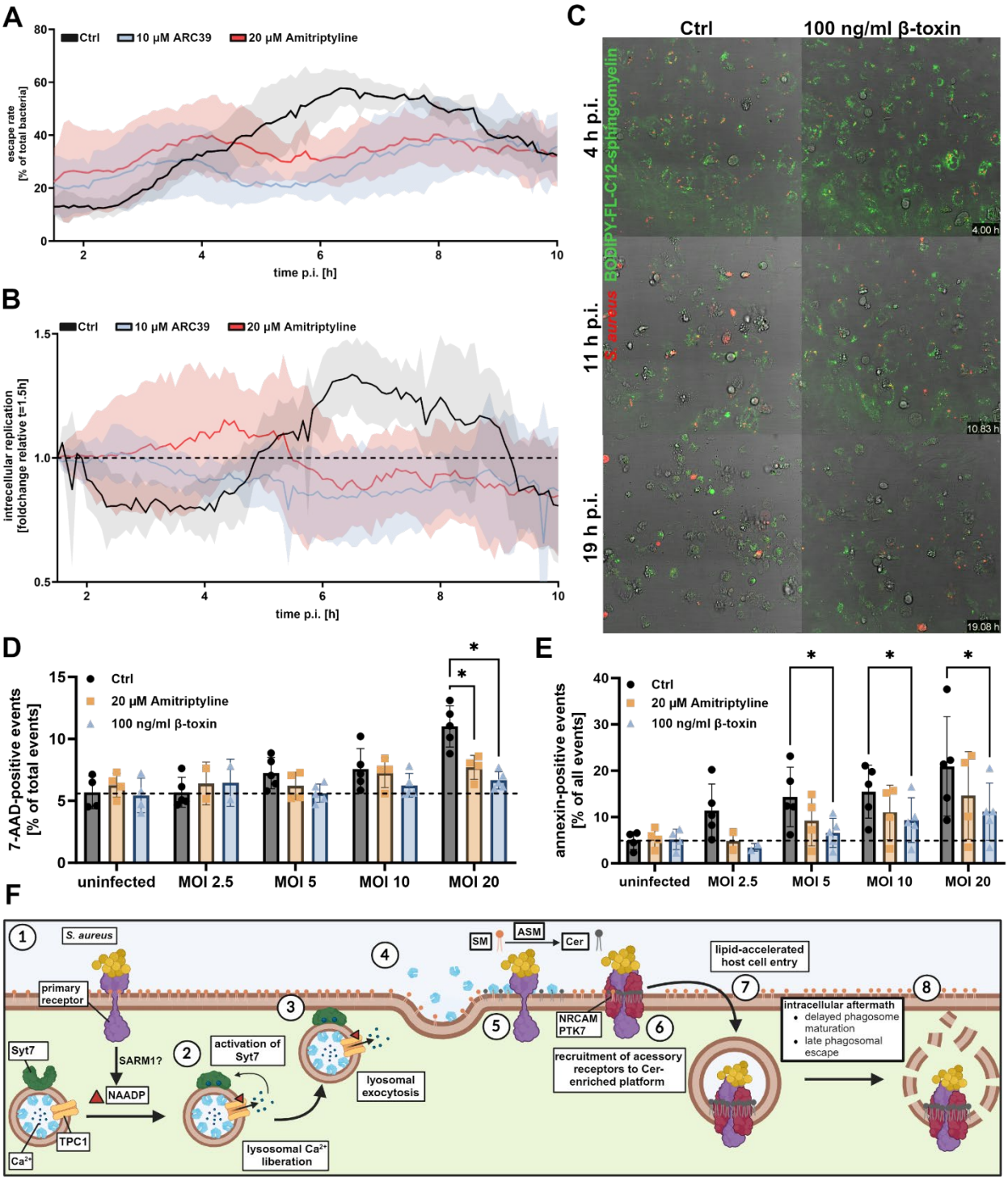

Figure 5 Blocking ASM-dependent internalization affects intracellular replication and host cell survival. **(A, B)** HeLa cells expressing RFP-CWT and Lysenin^{W20A}-YFP were treated with amitriptyline or ARC39 or were left untreated (Ctrl). The cells were subsequently infected with *S. aureus* and infection was monitored for 10 h by CLSM. Proportion of escaped bacteria (A) or the intracellular replication (B) was determined (n= 5). **(C)** HuLEC were stained with BODIPY-FL-C12-SM (green), and either were pretreated with 100 ng/ml of β-toxin or were left untreated. Then, cells were infected with *S. aureus* (red) and infection was monitored by CLSM for 19 h. **(D, E)** HuLEC were treated with amitriptyline or β-toxin and subsequently infected with *S. aureus*. After 21 h, plasma membrane integrity was measured by 7-AAD staining (D), and proportion of apoptotic cells was determined by annexin V staining (E) (n=5). See also **Supp. Figure 6**. (F) Model: *S. aureus* interacts with an unknown primary receptor (1) that triggers production of NAADP, which in turn activates TPC1 to mediate lysosomal Ca^{2+} release and activation of Syt7 (2). Syt7-dependent lysosomal exocytosis (3) leads to release of

330 ASM (4) and production of Cer on the plasma membrane (5) thereby resulting in the recruitment of co-receptors
331 (6) and rapid internalization of *S. aureus* by host cells (7). Bacteria that enter the host cells via the rapid pathway
332 experience a different intracellular fate than bacteria that entered via other pathways. **Statistics:** Mixed effects
333 analysis (REML) and Tukey‘s multiple comparison test. Graphs represent mean ± SD. *p≤0.05.
334
335 **Discussion**
336 ASM previously has been implicated in the invasion of several viral, bacterial, and eukaryotic pathogens
337 (5-11). However, the dynamics of ASM-mediated host cell entry, the underlying receptors as well as
338 effects on post-invasion events are only poorly understood.
339 We here show that ASM is involved within minutes after the pathogen contacts host cells and is
340 concurrent with ASM-independent uptake pathways. We demonstrate that the infection outcome of
341 bacteria that enter the host cells via this rapid pathway is distinct from other entry mechanisms.
342 We observed a reduction of bacterial invasiveness upon treatment with different ASM inhibitors (**Figure**
343 **2**, C, D) or removal of the enzyme substrate SM from the plasma membrane (**Figure 2**, E) confirming
344 that ASM activity on the host cell surface is crucial for pathogen internalization.
345 Release of ASM is caused by lysosomal exocytosis (56). Consequently, the inhibitor Vacuolin-1 as well
346 as genetic ablation of Syt7, a key protein in lysosomal exocytosis (55), resulted in drastically reduced
347 internalization of bacteria (**Figure 2**, A, B).
348 Elevation of cytosolic Ca^{2+} levels lead to recruitment of lysosomes to the cell surface (53). Whereas
349 most studies implicated Ca^{2+} influx from the extracellular milieu (8, 10), we here demonstrate that *S.*
350 *aureus* mainly triggers lysosomal Ca^{2+} mobilization as was shown by treatment with the inhibitor *trans*-
351 Ned19 as well as a genetic K.O. of the endo-lysosomal Ca^{2+} channel TPC1 (**Figure 1**, D and E; **Supp.**
352 **Figure 1**, G). TPCs have previously been associated with regulation of phagocytic processes (62) and
353 host cell entry of several viruses such as Ebola virus (63), Middle East respiratory syndrome coronavirus
354 [MERS-CoV, (64)] or SARS-CoV-II (65).
355 TPC-dependent Ca^{2+} liberation was shown to induce exocytosis, for instance, during release of cytolytic
356 granules from T cells (66) or in interplay with TRPM4 during secretion of insulin (67). Consistently, the
357 TRPM4 channel blocker 9-Phenantrol reduced internalization of *S. aureus* by host cells (**Figure 1**, B).
358 Interestingly, exogenous addition of a bacterial SMase immediately before infection rescued the
359 invasion defect in TPC1 and Syt7 K.O. cells (**Figure 2**, F) indicating that reduced invasion results from
360 a decreased delivery of ASM to the host cell surface. Thus, NAADP-dependent Ca^{2+} liberation from
361 lysosomal stores mediates Syt7-dependent fusion of lysosomes with the plasma membrane resulting in
362 the release of ASM (**Figure 5**, F).
363 Inhibition of CD38, a known NAADP producer (49, 50), did not influence uptake of staphylococci
364 (**Supp. Figure 1**, L). By contrast, we detected a decreased invasion in cells deficient for the Toll-like
365 receptor adaptor protein SARM1, an alternative NAADP producer (52). However, the role of SARM1
366 in lysosomal exocytosis and ASM release requires further investigation. The impact of SARM1 on
367 internalization of *S. aureus* was rather moderate, suggesting the existence of other NAADP-generating
368 enzymes.
369 One important characteristic of the ASM-dependent internalization pathway is its velocity - taking place
370 within the initial ten minutes of an infection with *S. aureus*, during which treatment with small molecules
371 (**Figure 3**, D), as well as genetic ablation of TPC1 (**Figure 1**, E) and Syt7 (**Figure 2**, B) resulted in
372 reduction of intracellular bacteria. This was accompanied by the quick formation of *S. aureus*-containing
373 phagosomes decorated with fluorescent SM analogs (**Figure 3**, A; **Supp. Figure 3**, **Supp. Video 1**,
374 **Supp. Video 2**).
375 When we blocked the rapid internalization pathway by ASM inhibitors (**Figure 4**, A, C; **Supp. Figure**
376 **4**, B), Vacuolin-1 (**Supp. Figure 4**, F) or by removal of surface SM (**Figure 4**, A, E; **Supp. Figure 4**, B,
377 H), we observed changes in both, maturation of bacteria-containing vesicles and phagosomal escape. A
378 delayed maturation of phagosomes may affect acidification of the vesicles, a property that is sensed by

S. aureus leading to expression of a different subset of virulence factors (68) and hence may alter intracellular pathogenicity. Phagosomal escape of *S. aureus* only was dependent on SM on the plasma membrane during invasion but not on the presence of SM within the phago-endosome (**Figure 4**, D-G; **Supp. Figure 4**, H, I). This not only corroborated that phagosomal escape of clinically relevant *S. aureus* strains is independent of the bacterial SMase β-toxin (36), but also demonstrated that the outcome of phagosomal escape is influenced by processes at the plasma membrane during cell entry.

To exclude that inhibitor or bSMase treatments caused changes in phagosomal escape by affecting cellular processes other than bacterial uptake, we infected untreated WT cells with *S. aureus* for 10 or 30 min, respectively, and monitored phagosomal escape. Bacteria that invaded within the first 10 minutes after contacting host cells ("early invaders") are predominantly ASM-dependent (**Figure 3**) and demonstrated significantly less phagosomal escape (**Figure 4**, G, H). Consistently, blocking the ASM-dependent pathway led to increased proportions of ASM-independent invaders, which in turn resulted in higher escape rates (**Figure 4**, C, E; **Supp. Figure 4**, F). Intracellular *S. aureus* infections thus are directly influenced by the mode of internalization. This ultimately resulted in lower host cytotoxicity (**Figure 5**, C-E; **Supp. Figure 6**) and bacterial replication (**Figure 5**, B) when we blocked the ASM-dependent invasion.

An uptake-related intracellular fate has been suggested for *Mycobacterium bovis* (39), *Toxoplasma gondii* (41) or *Brucella abortus* (42). However, in these studies the host cells were either depleted from cholesterol, which causes a variety of side effects (40), or internalization was artificially induced by chemicals or ectopic expression of receptors, respectively.

Taken together, we here describe a rapid internalization pathway for *S. aureus* into human epithelial and endothelial cells. Bacteria that enter the host cells via this infection route face a distinct intracellular fate. Here we show, to our knowledge, for the first time that host cells within the same population can be invaded by a pathogen via distinct routes and that this results in a differential infection outcome. Rapid internalization may prove beneficial for pathogens in an *in vivo* setting since internalization by host cells shortens the exposure to the innate immune system within a host. Interestingly, the absence of ASM in *Smpd1*$^{-/-}$ mice enhanced the potency of antibiotics to clear *S. aureus* sepsis (69). It is tempting to speculate that reduced host cell invasion in absence of ASM caused a prolonged exposure of the pathogen to antibiotics. Several FIASMAs are already approved drugs (70), and may have future use in infection treatment.

Acknowledgements:

This work was supported by the Deutsche Forschungsgemeinschaft (DFG; https://www.dfg.de) within the research training group RTG2581 (M.R., F.S.). C.K. and C.A. are grateful to the DFG AR 376/22-1. M.R. was supported by funds of the Bavarian State Ministry of Science and the Arts and the University of Würzburg to the Graduate School of Life Sciences (GSLS), University of Würzburg. The DFG funded the Leica TCS SP5 CLSM under project code 116162193 and the BD FACSAriaIII cell sorter under project code 206080318.

We thank Sibylle Schneider-Schaulies and Thomas Rudel for valuable discussions and critically reading the manuscript, and Nadine Vollmuth as well as Christian Stigloher for scientific advice and intense discussions. We are indebted to Kathrin Stelzner for conducting FACS of cell lines and generation of *S. aureus* strains. pmRFP-LC3 was a gift from Tamotsu Yoshimori (Addgene plasmid # 21075; http://n2t.net/addgene:21075; RRID:Addgene_21075, (71)). pLVTHM (72), pMD2.G and psPAX2 (unpublished) were a gift from Didier Trono (Addgene plasmids # 12247, 12259 and 12260, respectively). pLX304-Flag-APEX2-NES was a gift from Alice Ting (Addgene plasmid # 92158, (73)) and pSpCas9(BB)-p2A-GFP (PX458) (74) was a gift from Feng Zhang (Addgene plasmid # 48138; http://n2t.net/addgene:48138). Figures were created in BioRender.

Author Contributions:

M.R., M.F. conceptualized the work, designed the methodology and wrote the original draft manuscript. M.F. acquired funding. M.R. F.S., K.U., M.P., A.M., N.K., J.W., A.I., C.K., K.P. performed the experiments; M.R., M.F. supervised the experiments. M.R., C.A., M.F. analyzed the data; all authors edited and revised the manuscript.

Declaration of interests.

Patentability of PCK310 is currently evaluated by C.K. and C.A.

434 **Materials and Methods**

435 **Table 1 Oligonucleotides used in this study**

Purpose	Name	sequence (5´→ 3´)
Gene deletion	Syt7-sgRNA2 rv	AAACATGACGTCATTGCGGCTGAG
	Syt7-sgRNA2 fw	CACCCTCAGCCGCAATGACGTCAT
	Syt7-sgRNA1 rv	AAACCACGATGAGTCCGACCGCCG
	Syt7-sgRNA1 fw	CACCCGGCGGTCGGACTCATCGTG
	TPCN1-sgRNA2 rv	AAACAGGACGGCGCTCCTCATCTT
	TPCN1-sgRNA2 fw	CACCAAGATGAGGAGCGCCGTCCT
	TPCN1-sgRNA1 rv	AAACTTCAGACCCCGTAAGTAATC
	TPCN1-sgRNA1 fw	CACCGATTACTTACGGGGTCTGAA
	SARM1-sgRNA1 rv	AAACTAGAGTCGAGCAACGGCACG
	SARM1-sgRNA1 fw	CACCCGTGCCGTTGCTCGACTCTA
	SARM1-sgRN2 rv	AAACGCACGTAGAATAGTTGGCGA
	SARM1-sgRNA2 fw	CACCTCGCCAACTATTCTACGTGC
Cloning	MP-mRFP-f	GAGACTAGCCTCGAGGTTTAAACCACCATGGCCTCCTCCGAGGACGTC
	euk_mRFP-r	GGAATGCCCGGGCGCGCCGGTGGAGTGGCGGC
	infus-CWT-f	ACCGGCGCGCCCGGGCATTCCACGCCCAATACAGGTTGG
	infus-CWT-r	GAGGTTGATTATCATATGACTAGTTCACTTTATAGTTCCCCAAAG
	eYFP-rev	CTTGTTGATGGGCTCGAGCCCTTGTACAGCTCGTCCATGCCGAG
	Pm-eYFP-inf	GACTAGCCTCGAGGTTTAAACCACCATGGTGAGCAAGGGCGAGGAG
	hLysenin-infus-r	GAGGTTGATTATCATATGACTAGTTCAGCCCACCACCTCCAG
	InfReamp-f	GGCTCGAGCCCATCAACAAG
	cYFP-f	ATGGTGAGCAAGGGCGAGGAGCTG
	his1-Flag-f	CATCATCATCATCACGGAGCGGACTACAAGGATGACGACGATAAGG
	his2-Inf-f	GACTAGCCTCGAGGTTTAAACCACCATGGCACATCATCATCATCATCA CGGAGCG
	Apex-YFP-infus-r	CGCCCTTGCTCACCATCTCGAGCCGTCCAGGGTCAGGCGCTCC

436

437 **Cell culture**

438 HeLa (ATCC CCL-2™), 16HBE14o- (kindly provided by Prof. Jan-Peter Hildebrandt, University of
439 Greifswald) and EA.hy 926 (75) were cultivated in RPMI+GlutaMAX™ medium (Gibco™, Cat. No.
440 72400054) supplemented with 10% (v/v) heat-inactivated (56°C at 30 min) fetal bovine serum (FBS,
441 Sigma Aldrich, Cat. No. F7524) and 1 mM sodium pyruvate (Gibco™, Cat.No. 11360088).
442 HuLEC-5a (ATCC CRL-3244™) and HuVEC (Gibco™, Cat. No.C01510C) were cultured in
443 MCDB131 medium (Gibco™, Cat. No. 10372019) complemented with microvascular growth
444 supplement (Gibco™, Cat. No. S00525), 2 mM GlutaMAX™ (Gibco™, 35050061), 5 % (v/v) heat-
445 inactivated (56°C at 30 min) FBS, 2.76 µM hydrocortisone (Sigma Aldrich, Cat. No. H0888), 0.01 ng/ml
446 human epidermal growth factor (Pep Rotech, AF-100-15) and 1x Penicillin-Streptomycin (Gibco™, Cat.
447 No. 15140122).
448 HeLa
449 HuLEC and HuVEC were detached by StemPro™ Accutase™ (Gibco™, Cat. No. A1110501) and
450 seeded at the indicated density two days prior to the experiment, whereas HeLa, 16HBE14o- and EA.hy
451 926 were detached with TrypLE™ (Gibco™, Cat. No. 12604013) and seeded one day prior to the
452 experiment.
453
454

455 **Generation of HeLa KO cell lines.**
456 Generation of K.O. cell lines is based on a previous protocol (74). sgRNAs (**Table 1**) were designed
457 with the CHOPCHOP online tool (chopchop.cbu.uib.no) and synthesized as primer pairs (Sigma
458 Aldrich). After phosphorylation with T4 nucleotide kinase (ThermoFisher, Cat. No. ER0031), the
459 sgRNAs were cloned into the BbsI sites of pSpCas9(BB)-p2A-GFP (AddGene #48138, (74)) via forced
460 ligation by BbsI (ThermoFisher, Cat. No. ER1012) and T4 Nulceotide ligase (ThermoFisher, Cat. No.
461 EL0011). The constructs were then transformed in *E. coli* DH5α (ThermoFisher, Cat. No EC0112) and
462 subsequently sequence verified.
463 HeLa cells were transfected with 1 µg each of two distinct sgRNA constructs using JetPrime (Polyplus)
464 following the manufacturer's instructions. After 36-48h, cells were sorted for strong GFP expression in
465 a FACS Aria III (BD Bioscience). The resulting cell pools were cultivated and tested for loss of
466 expression of the respective sgRNA target by Western Blotting.
467 Following antibodies were used: mouse anti-PTK7 monoclonal IgG1 (bio-techne, Cat. No.
468 MAB4499) with a horse radish peroxidase (HRP)-conjugated anti-mouse antibody (SantaCruz, Cat. No.
469 sc-516102) and rabbit anti-TPC1 polyclonal (Thermo Fisher, Cat. No. PA5-41048) with an HRP-
470 conjugated anti-rabbit antibody (Biozol, Cat. No. 111-035-144).
471

472 **Generation of reporter constructs.**
473 *pLV-mRFP-CWT.* mRFP and the cell wall-targeting domain of lysostaphin CWT were amplified using
474 primers MP-mRFP-f and euk_mRFP-r, as well as infus-CWT-f and infus-CWT-r, respectively. As PCR
475 templates we used pmRFP-LC3 (PMID 17534139) and pLV-YFP-CWT (76). The resulting plasmid was
476 termed pLV-mRFP-CWT. The PCR products were subsequently cloned into pLVTHM (72) restricted
477 with PmeI and SpeI by InFusion cloning following the manufacturer's recommendations.
478
479 *pLV-YFP-Lysenin.* The sequence of the sphingomyelin-binding but not pore-forming earthworm toxin
480 mutant Lysenin^{W20A} (61) was synthesized by GeneArt (ThermoFisher) using a human codon usage and
481 5' flanking region encoding a glycine-rich linker sequence. The synthesized template served as template
482 for subsequent PCRs.
483 Lysenin^{W20} was amplified using oligonucleotides InfReamp-f and hLysenin-infus-r (**Table 1**).
484 YFP was amplified with Pm-eYFP-inf and eYFP-rev from template pLVTHM-YFP-CWT (76). Both
485 PCR products were joined with pLVTHM vector restricted with PmeI and SpeI by InFusion cloning
486 following the manuacturer's recommendations, thereby creating pLV-YFP-Lysenin.
487
488 Constructs were transformed into *E. coli* DH5α and sequences were validated. Plasmid preparations
489 were performed using standard laboratory procedures. VSV-G-pseudotyped Lentiviral particles were
490 generated by transfecting with each lentiviral vector as well as the plasmids pMD2.G (VSV G) and
491 psPAX2 following the protocol of (72) and target cells were transduced as described previously (76).
492
493 ***S. aureus* culture**
494 *S. aureus* liquid cultures were either grown in 37 g/L brain heart infusion (BHI) medium (Thermo Fisher,
495 Cat. No. 237300) or in 30 g/l TSB medium (Sigma Aldrich, Cat. No. T8907). *E. coli* liquid cultures
496 were grown in LB medium [10 g/l tryptone/peptone (Roth, Cat. No. 8952.4,) 5g/l yeast extract (Roth,
497 Cat. No 2363.2), 10 g/l NaCl (Sigma Aldrich, Cat. No. S5886)].
498 For agar plates, 15 g/L agar (Otto Norwald, Cat. No. 257353), was added to either TSB (*S. aureus*) or
499 LB (E. coli).
500 Media and plates were supplemented with appropriate antibiotics [5 µg/ml erythromycin (Sigma
501 Aldrich, Cat. No. E5389), 10 µg/ml chloramphenicol (Roth, Cat. No. 3886.2), 100 ng/ml Carbenicillin
502 (Roth, Cat. No. 6344.2)].

503 Strains used in this study are listed in **Table 2**.
504

505 **Table 2 Bacterial Strains used in this study**

Strain	Remarks	Source
S. aureus 6850		(77)
S. aureus 6850 Δ*hlb*	deficient in β-toxin production	(36)
S. aureus Cowan I	NCTC 8530, isolated from septic arthritis, agr dysfunction, low expression of toxins and proteases	ATCC 12598
S. aureus JE2	MRSA, USA300	(78)
S. aureus JE2 Δ*hla*	deficient in α-toxin production	(79)
S. aureus JE2 Δ*hlb*	deficient in β-toxin production	(45)
S. aureus JE2 SarAP1 Cerulean	Constitutive expression of the fluorescence protein Cerulean	This work
S. aureus JE2 SarAP1 mRFP	Constitutive expression of the fluorescence protein mRFP	(38)
S. aureus JE2 p*Cer*	Anhydrous tetracycline (AHT) inducible expression of Cerulean, construct published in (80) and was transduced into *S. aureus* JE2	This work
S. aureus JE2 p*Cer+hlb*	Anhydrous tetracycline (AHT) inducible expression of Cerulean and β-toxin, construct published in (80) and was transduced into *S. aureus* JE2	This work
S. aureus Cowan I *SarAP1 Cerulean*	Constitutive expression of the fluorescence protein Cerulean	This work
S. aureus 6850 SarAP1 Cerulean	Constitutive expression of the fluorescence protein Cerulean	(38)
S. aureus 6850 Δ*hlb* SarAP1 Cerulean	Constitutive expression of the fluorescence protein Cerulean	This work

506
507
508 ***S. aureus* growth curves**
509 *S. aureus* overnight cultures were grown in BHI medium, and 1 ml was centrifuged at 14,000 for 1 min.
510 Bacteria were washed thrice with DPBS and either resuspended in BHI (for amitriptyline and ARC39
511 treatment) or infection medium [MCDB131 medium (Gibco™, Cat. No. 10372019) complemented with
512 2 mM GlutaMAX™ (Gibco™, 35050061) and 10 % (v/v) heat-inactivated (56°C at 30 min) FBS, for
513 ionomycin treatment). Bacteria suspensions were diluted to OD_{600}=0.1 in the respective medium. Then,
514 400 µL per well of the suspension as well as respective blanks were transferred into a 48 well plate and
515 OD_{600} was determined every 16 min in Tecan mPlex200 microplate reader.
516 ***S. aureus* infections**
517 Host cells were seeded in 6 well plates ($2x10^5$ cells per well), 12 well plates ($1x10^5$ cells per well) or 24
518 well plates ($0.5x10^5$ cell per well) either one day (HeLa, EA.hy 926, 16HBE14o$^-$) or two days (HuLEC,
519 HuVEC) prior to the experiment. Host cells were washed thrice with DPBS and infection medium or
520 Ca^{2+}-free infection medium [DMEM w/o calcium (Gibco™, Cat. No. 21068028) complemented with
521 10 % (v/v) heat-inactivated (56°C at 30 min) FBS and 200 µM BAPTA (Merck Millipore, 196418)]
522 with or without 1.8 mM $CaCl_2$ (Roth, Cat. No. 5239.1) was added. If indicated, cells were pretreated
523 with compounds prior to infection (for details about treatments see **Table 1**). For experiments involving
524 blocking of receptors by antibodies, respective solvent controls were implemented (final concentrations
525 in infection medium: 0.002% (w/v) NaN_3 (Sigma Aldrich, Cat. No. S2002) 5% glycerol (Roth, Cat. No

526 3783.2) in 10% DPBS for 30 ng/ml anti-NRCAM antibody as well as well as 0.01 % (w/v) NaN_3 for
527 50 ng/ml anti-CD73 and 50 ng/ml anti-MELTF antibodies.
528
529 **Table 3 Host cell treatment with various compounds**

compound	Supplier/Cat.No.	preincubation time	removal prior to infection?
2-APB (2-Aminoethoxydiphenylborate)	Sigma Aldrich/ D9754	75 min	removed prior to infection
8-Bromo-cADPR (8-Bromo-cyclic ADP ribose)	Biolog/065-005	75 min	present during infection
9-Phenantrol	Biomol/ Cay15248-50	75 min	present during infection
amitriptyline	Sigma Aldrich/ A8404	75 min	present during infection
ARC39	(57)	18 h, add fresh inhibitor for another 4h or as indicated	present during infection
BAPTA-AM	Merck Millipore/ 196419; (44)	25 min	removed prior to infection
BODIPY-FL™-C12-Ceramide	Santa Cruz/ sc-503923	90 min	present during infection
BODIPY-FL™-C12-Sphingomyelin	ThermoFisher/D7711	90 min	present during infection
CD38i/78c	Sigma Aldrich/ 5387630001	75 min	present during infection
Ionomycin	Sigma Aldrich/ I0634	75 min	present during infection
PCK310	To be published elsewhere	4h or as indicated	present during infection
trans-Ned19	Sigma Aldrich/ SML2830; (48)	75 min	present during infection
Vacuolin-1	Biozol/ MCE-HY-118630	75 min	present during infection
β-toxin	Sigma Aldrich/ S8633	75 min	removed prior to infection if not indicated otherwise

530
531 An *S. aureus* overnight culture grown in BHI containing the appropriate antibiotics was diluted to an
532 OD_{600}=0.4 in the same medium. When inducible expression of genes was required for the strains *S.*
533 *aureus* JE2 p*Cer* and *S. aureus* JE2 p*Cer+hlb,* 200 ng/ml anhydrous tetracycline (AHT, AcrosOrganics,
534 233131000) was added. The culture was grown to an OD_{600}= 0.6-1.0 and 1 ml bacterial suspension was
535 harvested by centrifugation and washed twice with Dulbecco's Phosphate Buffered Saline (DPBS,
536 Gibco™, Cat. No 14190169). The bacteria were resuspended in infection medium (or Ca^{2+}-free infection
537 medium when infection was performed in absence of extracellular Ca^{2+}). The number of bacteria per ml
538 in the suspension was determined with a Thoma counting chamber and the MOI was determined. If not
539 indicated otherwise, an MOI=10 was used for infections.

540 The infection was synchronized by centrifugation 800xg/8 min/RT (end of the centrifugation: t=0). To
541 determine bacterial invasion, the infection was stopped after 30 min (unless indicated otherwise) by
542 removing extracellular bacteria with 20 µg/ml Lysostaphin (AMBI, Cat. No. AMBICINL) in infection
543 medium for 30 min. Then, host cells were washed thrice with DPBS, lysed by addition of 1 ml/well (12
544 well plate) or 0.5 ml/well (24 well plate) Millipore water and the number of bacteria in lysates was
545 determined by plating serial dilutions (10^{-1}, 10^{-2}, 10^{-3}) on TSB agar plates. Plates were incubated
546 overnight at 37 °C and CFU were enumerated. To determine invasion efficiency, the number of bacteria
547 determined in tested samples were normalized to untreated controls (set to 100%).
548 For measuring invasion dynamics, the number of bacteria was either normalized to the 30 min time point
549 of untreated controls or to the corresponding time points of untreated controls.
550 If later time points in infection were investigated, infection medium containing 2 µg/ml Lysostaphin
551 was added to the cells until the indicated time.
552 For testing bacterial susceptibility to inhibitors ("survival") or adherence, Lysostaphin treatment was
553 omitted, and host cells were immediately lysed by addition of Millipore water or washed five times with
554 DPBS and subsequently lysed with Millipore water, respectively. The number of bacteria in lysates was
555 determined by CFU counting (dilutions 10^{-2}, 10^{-3}, 10^{-4}) on TSB agar plates.
556
557 **Phagosomal escape assays**
558 For phagosomal escape assays with amitriptyline, ARC39, PCK310 and β-toxin, HeLa cells expressing
559 RFP-CWT and Lysenin^{W20A}-YFP were infected with the indicated *S. aureus* strain as described in the
560 previous paragraph. Infections with *S. aureus* JE2 p*Cer* and *S. aureus* JE2 p*Cer+hlb* were carried out in
561 presence of 200 ng/ml AHT.
562 For phagosomal escape assays, HeLa cells expressing RFP-CWT and Lysenin^{W20A}-YFP were infected
563 for 10 min (early invaders) or 30 min (early and late invaders) at the indicated MOIs.
564 For the phagosomal escape assays with two *S. aureus* JE2 strains expressing different fluorescence
565 proteins, HeLa cells expressing YFP-CWT were infected with an MOI=5 of an initial *S. aureus* JE2
566 strain (*S. aureus* JE2 SarAP1 Cerulean or *S. aureus* JE2 SarAP1 mRFP). After 12 min of infection, a
567 second infection pulse was initiated by adding the second *S. aureus* JE2 strain (expressing the
568 complementary fluorescence protein, *S. aureus* JE2 SarAP1 mRFP or *S. aureus* JE2 SarAP1 Cerulean,
569 respectively) and centrifuging the bacteria on the host cells. To exclude that the type of fluorescence
570 protein expressed by the *S. aureus* strains contributes to the experimental outcome, either strain was
571 used for the first and second infection pulse (each combination: n=4).
572
573 **Phagosomal maturation assays**
574 To monitor phagosomal maturation, HeLa cells expressing mCherry-Rab5 and YFP-Rab7 or YFP-Rab7
575 and RFP-CWT were infected with *S. aureus* JE2 SarAP1 Cerulean.
576 After 3 h p.i. (unless indicated otherwise), cells were washed thrice with DPBS and fixed with 0.2%
577 glutaraldehyde (Sigma Aldrich, Cat. No. 10333) / 4% paraformaldehyde in PBS (Morphisto, Cat. No
578 11762.01000) for 30 min at RT. Then, cells were washed thrice with DPBS, stained with 5µg/ml Hoechst
579 34580 (Thermo Fisher, Cat. No. H21486) and mounted in Mowiol [24g glycerol (Roth, Cat. No. 3783.2),
580 9.6 g Mowiol®4-88 (Roth, Cat. No 0713.2), 48 ml 0.2 M TRIS-HCl pH 8.5 (Sigma Aldrich, Cat. No
581 T1503), 24 ml Millipore water].
582 Samples were imaged with a Leica TCS SP5 confocal microscope (Wetzlar, Germany; Software Leica
583 LAS AF Version 2.7.3.9723) with a 40x immersion oil objective (NA1.3) and a resolution of 1024x1024
584 pixels [Cerulean (Ex. 458 nm/Em. 460-520), YFP (Ex. 514 nm/Em. 520-570nm), mRFP/mCherry (Ex.
585 561 nm/Em.571-635nm) and Hoechst 34580 (Ex. 405 nm/Em.410-460nm). At least 10 fields of view
586 per samples were recorded.
587 Image analysis was performed in Fiji (81) using a previously described macro (80) that identifies and
588 extracts individual bacteria from images as regions of interest (ROIs, see **Supp. Figure 5**).

589 Subsequently, fluorescent intensity in every channel is measured to determine recruitment of
590 fluorescence reporters to the bacteria. Results were exported as text files and proportion of bacteria that
591 recruited individual reporters was determined with the Flowing 2 software (Turku Bioscience Center).
592 Phagosomal escape rates were determined as the proportion of CWT-positive bacteria of the total
593 number of intracellular bacteria. Similarly, the proportion of Lysenin^{W20A}-positive escape events, the
594 ratio of Lysenin^{W20A}-/CWT-positive events and all CWT-positive events was calculated.
595 To measure the proportion of bacteria that were associated with Rab5 and/or Rab7, the proportion of
596 Rab5- and/or Rab7-positive membranes around bacteria of all intracellular bacteria was determined. For
597 experiments obtained with HeLa cells expressing YFP-Rab7 and RFP-CWT, bacteria that acquired RFP-
598 CWT were removed from the dataset. Subsequently, the proportion of Rab7-positive bacteria in relation
599 to all CWT-negative intracellular bacteria was determined.
600
601 **Live cell imaging**
602 The indicated host cells were seeded one (HeLa) or two days (HuLEC) prior to the experiments in µ-
603 slide 8 well live cell chambers (ibidi, Cat. No 80826-90) with a density of $0.375x10^5$ cells per well.
604 For monitoring host cell entry, cells were washed thrice with DPBS and were then, incubated for 90 min
605 in infection medium with 1 µM BODIPY-FL-C_{12}-sphingomyelin (Thermo Fisher Cat. No. D7711), 10
606 µM BODIPY-FL-C_{12}-ceramide (Santa Cruz, Cat.No. sc-503923) or 10 µM visible-range FRET probe
607 (59). Pretreatment with the FRET probe was performed in infection medium containing 1 % (v/v) FBS.
608 Then, cells were washed thrice with DPBS and imaging medium [RPMI 1640 w/o phenol red (Gibco™,
609 Cat. No. 11835030) containing 10% (v/v) heat-inactivated (56°C/30 min) FBS (Sigma Aldrich, Cat. No.
610 F7524) and 30 mM HEPES (Gibco™, Cat.No. 15630080)] applied. Samples stained with the FRET
611 probe were imaged in imaging medium containing 1% FBS and in presence of 10 µM FRET probe.
612 Samples were infected with *S. aureus* JE2 SarAP1 Cerulean (FRET probe samples) or *S. aureus* JE2
613 SarAP1 mRFP (BODIPY-FL-C12-sphingomylein/-ceramide) at an MOI=50 without synchronization
614 by centrifugation. Infection was monitored with a Leica TCS SP5 confocal microscope (Wetzlar,
615 Germany) in intervals of 1 min by recording BODIPY-FL (Ex. 496 nm/Em. 500-535 nm), mRFP (Ex.
616 561 nm/Em.571) FITC (Ex. 488 nm/Em. 500-560), Cerulean (Ex. 458 nm/Em. 460-520), BODIPY-TR
617 (Ex. 594 nm/Em. 610-680) and FRET (Ex.488 nm/ Em:610-680) channels. Cells were recorded with a
618 40x immersion oil objective and a resolution of 2048x2048 pixels. For samples stained with the FRET
619 probe, 20 µg/ml lysostaphin was added 40 min p.i. to remove extracellular bacteria.
620 For quantification of bacteria that associate with BODIPY-FL-C_{12}-sphingomyelin/-ceramide, individual
621 bacteria in single frames were identified, extracted as ROIs and BODIPY-FL fluorescence in ROIs was
622 measured in Fiji (81) as described before for phagosomal escape assays. Results were extracted as text
623 files and the proportion of bacteria associating with BODIPY-FL was determined with Flowing2 (Turku
624 Bioscience Center).
625 For monitoring intracellular *S. aureus* infection, host cells were pretreated and infected with
626 *S. aureus* JE2 SarAP1 Cerulean (HeLa RFP-CWT/Lysenin^{W20A}-YFP) or *S. aureus* JE2 SarAP1 mRFP
627 (HuLEC) as described in "*S. aureus* infection". HuLEC additionally were treated with 1 µM BODIPY-
628 FL-C_{12}-sphingomyelin in infection medium for 90 min and washed thrice with DPBS before the
629 indicated treatment was applied. After extracellular bacteria were removed with 20 µg/ml lysostaphin
630 for 30 min, imaging medium containing 2 µg/ml lysostaphin was applied and infections were monitored
631 in intervals of 5 min (HeLa RFP-CWT) or 20 min (HuLEC). Phagosomal escape was evaluated in Fiji
632 as described above. To determine intracellular replication, the number of bacteria was determined for
633 each individual frame as described before (80). The number of bacteria at each time point was then
634 normalized to the number of bacteria detected in the first frame to calculate the relative replication.
635
636
637

638 **ASM and NSM activity assays**
639 Thin layer chromatography (TLC)-based ASM/NSM activity assays were adapted from previously
640 published protocols (58). To determine cellular ASM activity, the indicated cell lines were seeded in 24
641 well plates with a density of $1x10^5$ cell per well one day (HeLa, EA.hy 926, 16HBE14o$^-$) or two days
642 (HuLEC, HuVEC) prior to the experiment. Cells were either treated with 20 µM amitriptyline or with
643 10 µM ARC39 for 22 h (fresh inhibitor was applied after 18h) in infection medium. Then, cells were
644 washed thrice and lysed by addition of 100 µL per well ASM lysis buffer [250 mM NaOAc pH 5 (Roth,
645 Cat. No 6773.2), 0.1% Nonidet® P40 substitute (AppliChem. Cat. No. A1694,0250), 1.3 mM EDTA 1.3
646 mM (Roth, Cat. No. 8040.2), 1x protease inhibitor cocktail (Sigma Aldrich, 11873580001)] for 15
647 min/4°C. Cells were scraped from the substratum and protein concentration in the resulting lysates was
648 measured with a Pierce™ bicinchoninic acid (BCA) assay kit (Thermo Fisher, Cat. No. 23227). 1 µg of
649 protein was incubated with 100 µL ASM lysate assay buffer [200 mM NaOAc pH 5 (Roth, Cat. No
650 6773.2), 0.02 % Nonidet® P40 substitute (AppliChem. Cat. No. A1694,0250), 500 mM NaCl (VWR,
651 Cat. No. 27810.364)] containing 0.58 µM BODIPY-FL-C_{12}-Sphingomyelin (Thermo Fisher, Cat. No.
652 D7711) for 4h at 37°C and 300 rpm.
653 For measuring bacterial SMase/NSM activity in *S. aureus* cultures, an overnight culture of the indicated
654 strain was grown in BHI medium, centrifuged 14.000xg and the supernatant was sterile filtered with 0.2
655 µm filter. 100 µL of sterile supernatant was incubated with 100 µL NSM assay buffer [200 mM HEPES,
656 pH 7.0 (Roth, Cat. No. 6763.3), 200 mM $MgCl_2$ (Roth, Cat.No. 2189.2), 0.05% Nonidet P-40
657 (AppliChem. Cat. No. A1694,0250)] for 4h/37°C/300 rpm.
658 The reactions were stopped by addition of 2:1 $CHCl_3$:MeOH (Roth, Cat. No. 3313.2 and Cat. No.
659 8388.6). Samples were vortexed, centrifuged at 13,000 x g for 3 min and 50-100 µL of the lower organic
660 phase were transferred to a fresh tube. Samples were completely evaporated using a SpeedVac 5301
661 concentrator (Eppendorf), resuspended in 10 µL 2:1 $CHCl_3$/MeOH and spotted in 2.5 µL aliquots on a
662 TLC plate (Alugram, Xtra Sil G/UV254, 0.2 mm/silica gel 60; VWR, Cat. No. 552-1006).
663 Plates were developed using 80:20 $CHCl_3$ and subsequently scanned with a Typhoon 9200 Scanner
664 (Amersham). For quantification, intensities of the lower (SM) and the upper bands (Cer) were measured
665 in Fiji (81) and activity was determined based on the reaction time, protein amount and SM/Cer ratios.
666 For the flow cytometry based read out, cells seeded in a density of $0.5x10^5$ cells per well in a 24 well
667 plate either one day (HeLa, EA.hy 926, 16HBE14o$^-$) or two days (HuLEC, HuVEC) prior to the
668 experiment. Cells were treated with ARC39 and amitriptyline as described above. Then, cells were
669 washed thrice with DPBS and incubated with 10 µM FRET probe (59) for 2h in presence of the
670 inhibitors. Subsequently, cells were washed thrice, detached with TrypLE™ (Gibco™, Cat. No.
671 12604013) and resuspended with 2% (v/v) FBS in DPBS. Samples were analyzed for FITC (Ex. 488
672 nm/Em. band pass 530/30 nm) and BODIPY-TR (Ex.: 561nm/ Em. band pass 695/40nm) fluorescence
673 with Attune NxT flow cytometer (Thermo Fisher, Attune Cytometric Software v5.2.0). Cell populations
674 were analyzed for FITC and BODIPY-TR mean fluorescence in Flowing 2 (Turku Bioscience Center)
675 and FITC vs. BODIPY-TR ratios were calculated to determine arbitrary probe conversion.
676
677 **Cytotoxicity Assays**
678 For all cytotoxicity assays, HuLEC were seeded in 24 well plates with a density of $0.5x10^5$ cells per
679 well two days prior to the experiment. Then, cells were infected with *S. aureus* JE2 with the indicated
680 MOI as described in "*S. aureus* infection" and cytotoxicity was determined 21 h p.i. For cytotoxicity
681 measurements upon ionomycin treatment, cells were incubated with the indicated concentration of
682 ionomycin in infection medium for 75 min and then, cytotoxicity assays were conducted.
683 Lactate dehydrogenase (LDH) assay was performed with the Cytotoxicity Detection KitPLUS (LDH,
684 Sigma Aldrich, Cat. No. 4744934001) according to manufacturer's instructions.
685 For annexin V and 7-Aminoactinomycin D (7-AAD) assays, cells were washed thrice with DPBS,
686 detached with 250 µL per well trypsin and resuspended in 250 µL per well staining buffer [1.7% (v/v)

687 APC Annexin V (BD Pharmingen™, Cat. No. 550475), 1.7% (v/v) 7-AAD (BD Pharmingen™, Cat No.
688 559925), 2% (v/v) heat-inactivated (56°C/30 min) FBS (Sigma Aldrich, Cat. No. F7524), 4 mM $CaCl_2$
689 (Roth, Cat. No. 5239.1) in DPBS]. After incubation for 10 min/RT, cells were analyzed with a Attune
690 NxT flow cytometer for 7-AAD (Ex. 488 nm/Em. band pass 695/40 nm) and APC (Ex. 637 nm/Em.
691 band pass 670/14 nm). Cell populations were analyzed with Flowing2 (Turku Biosciences Center) and
692 gates were adjusted according to untreated control cells. To determine the proportion of cells that
693 remained attached to the substratum during the infection, number of cells was determined based on the
694 number of detected single cells, flow rate and sample volume.
695
696 **Statistical analysis**
697 Statistical analysis was performed in GraphPad prism (V10.1.2). One-sample t-test was used for analysis
698 of normalized data sets. Otherwise, one- or two-way ANOVA, dependent on the number of variables,
699 was used in combination with suitable multiple comparisons testing. Details about sample size and
700 deployed statistical analysis can be found in respective figure legends. All data are shown as mean ±
701 standard deviation.
702
703

704 **References**

705 1. G. van Meer, D. R. Voelker, G. W. Feigenson, Membrane lipids: where they are and how they
706 behave. *Nat Rev Mol Cell Biol* **9**, 112-124 (2008).
707 2. K. Segawa, J. Suzuki, S. Nagata, Flippases and scramblases in the plasma membrane. *Cell Cycle*
708 **13**, 2990-2991 (2014).
709 3. R. O. Brady, J. N. Kanfer, M. B. Mock, D. S. Fredrickson, The metabolism of sphingomyelin. II.
710 Evidence of an enzymatic deficiency in Niemann-Pick diseae. *Proc Natl Acad Sci U S A* **55**, 366-
711 369 (1966).
712 4. B. Breiden, K. Sandhoff, Acid Sphingomyelinase, a Lysosomal and Secretory Phospholipase C, Is
713 Key for Cellular Phospholipid Catabolism. *Int J Mol Sci* **22** (2021).
714 5. C. Li *et al.*, Regulation of Staphylococcus aureus Infection of Macrophages by CD44, Reactive
715 Oxygen Species, and Acid Sphingomyelinase. *Antioxid Redox Signal* **28**, 916-934 (2018).
716 6. S. Peters *et al.*, Neisseria meningitidis Type IV Pili Trigger Ca(2+)-Dependent Lysosomal
717 Trafficking of the Acid Sphingomyelinase To Enhance Surface Ceramide Levels. *Infect Immun* **87**
718 (2019).
719 7. H. Grassme *et al.*, Acidic sphingomyelinase mediates entry of N. gonorrhoeae into
720 nonphagocytic cells. *Cell* **91**, 605-615 (1997).
721 8. M. C. Fernandes *et al.*, Trypanosoma cruzi subverts the sphingomyelinase-mediated plasma
722 membrane repair pathway for cell invasion. *J Exp Med* **208**, 909-921 (2011).
723 9. A. Carpinteiro *et al.*, Pharmacological Inhibition of Acid Sphingomyelinase Prevents Uptake of
724 SARS-CoV-2 by Epithelial Cells. *Cell Rep Med* **1**, 100142 (2020).
725 10. S. Luisoni *et al.*, Co-option of Membrane Wounding Enables Virus Penetration into Cells. *Cell*
726 *Host & Microbe* **18**, 75-85 (2015).
727 11. E. Avota, E. Gulbins, S. Schneider-Schaulies, DC-SIGN mediated sphingomyelinase-activation
728 and ceramide generation is essential for enhancement of viral uptake in dendritic cells. *PLoS*
729 *Pathog* **7**, e1001290 (2011).
730 12. A. Sakr, F. Brégeon, J. L. Mège, J. M. Rolain, O. Blin, Staphylococcus aureus Nasal Colonization:
731 An Update on Mechanisms, Epidemiology, Risk Factors, and Subsequent Infections. *Front*
732 *Microbiol* **9**, 2419 (2018).
733 13. L. F. McCaig, L. C. McDonald, S. Mandal, D. B. Jernigan, Staphylococcus aureus-associated skin
734 and soft tissue infections in ambulatory care. *Emerg Infect Dis* **12**, 1715-1723 (2006).
735 14. L. Liesenborghs *et al.*, Staphylococcus aureus endocarditis: distinct mechanisms of bacterial
736 adhesion to damaged and inflamed heart valves. *Eur Heart J* **40**, 3248-3259 (2019).
737 15. J. A. Silversides, E. Lappin, A. J. Ferguson, Staphylococcal toxic shock syndrome: mechanisms
738 and management. *Curr Infect Dis Rep* **12**, 392-400 (2010).
739 16. C. Antimicrobial Resistance, Global burden of bacterial antimicrobial resistance in 2019: a
740 systematic analysis. *Lancet* **399**, 629-655 (2022).
741 17. M. Fraunholz, B. Sinha, Intracellular Staphylococcus aureus: live-in and let die. *Front Cell Infect*
742 *Microbiol* **2**, 43 (2012).
743 18. I. Rodrigues Lopes *et al.*, Microscopy-based phenotypic profiling of infection by Staphylococcus
744 aureus clinical isolates reveals intracellular lifestyle as a prevalent feature. *Nature*
745 *Communications* **13**, 7174 (2022).
746 19. J. W. Hommes, B. G. J. Surewaard, Intracellular Habitation of Staphylococcus aureus: Molecular
747 Mechanisms and Prospects for Antimicrobial Therapy. *Biomedicines* **10**, 1804 (2022).
748 20. S. N. Qazi, S. E. Harrison, T. Self, P. Williams, P. J. Hill, Real-time monitoring of intracellular
749 Staphylococcus aureus replication. *J Bacteriol* **186**, 1065-1077 (2004).
750 21. J. Abel *et al.*, Staphylococcus aureus evades the extracellular antimicrobial activity of mast cells
751 by promoting its own uptake. *J Innate Immun* **3**, 495-507 (2011).
752 22. B. Sinha *et al.*, Fibronectin-binding protein acts as Staphylococcus aureus invasin via fibronectin
753 bridging to integrin alpha5beta1. *Cell Microbiol* **1**, 101-117 (1999).

754 23. F. Agerer *et al.*, Cellular invasion by Staphylococcus aureus reveals a functional link between
755 focal adhesion kinase and cortactin in integrin-mediated internalisation. *J Cell Sci* **118**, 2189-
756 2200 (2005).
757 24. F. Agerer, A. Michel, K. Ohlsen, C. R. Hauck, Integrin-mediated invasion of Staphylococcus
758 aureus into human cells requires Src family protein-tyrosine kinases. *J Biol Chem* **278**, 42524-
759 42531 (2003).
760 25. Y. T. Ying *et al.*, Annexin A2-Mediated Internalization of Staphylococcus aureus into Bovine
761 Mammary Epithelial Cells Requires Its Interaction with Clumping Factor B. *Microorganisms* **9**
762 (2021).
763 26. S. L. Stroschein-Stevenson, E. Foley, P. H. O'Farrell, A. D. Johnson, Identification of Drosophila
764 gene products required for phagocytosis of Candida albicans. *PLoS Biol* **4**, e4 (2006).
765 27. A. M. Towell *et al.*, Staphylococcus aureus binds to the N-terminal region of
766 corneodesmosin to adhere to the stratum corneum in atopic dermatitis. *Proceedings of the*
767 *National Academy of Sciences* **118**, e2014444118 (2021).
768 28. F. Askarian *et al.*, The interaction between Staphylococcus aureus SdrD and desmoglein 1 is
769 important for adhesion to host cells. *Scientific Reports* **6**, 22134 (2016).
770 29. N. Bravo-Santano *et al.*, Host-directed kinase inhibitors act as novel therapies against
771 intracellular Staphylococcus aureus. *Scientific Reports* **9**, 4876 (2019).
772 30. P. M. Tribelli *et al.*, Staphylococcus aureus Lpl protein triggers human host cell invasion via
773 activation of Hsp90 receptor. *Cell Microbiol* **22**, e13111 (2020).
774 31. N. Hirschhausen *et al.*, A novel staphylococcal internalization mechanism involves the major
775 autolysin Atl and heat shock cognate protein Hsc70 as host cell receptor. *Cell Microbiol* **12**,
776 1746-1764 (2010).
777 32. K. Dziewanowska *et al.*, Staphylococcal fibronectin binding protein interacts with heat shock
778 protein 60 and integrins: role in internalization by epithelial cells. *Infect Immun* **68**, 6321-6328
779 (2000).
780 33. A. Moldovan, M. J. Fraunholz, In or out: Phagosomal escape of Staphylococcus aureus. *Cell*
781 *Microbiol* **21**, e12997 (2019).
782 34. C. E. Jauregui, J. P. Mansell, M. A. Jepson, H. F. Jenkinson, Differential interactions of
783 Streptococcus gordonii and Staphylococcus aureus with cultured osteoblasts. *Mol Oral*
784 *Microbiol* **28**, 250-266 (2013).
785 35. B. Giese *et al.*, Staphylococcal alpha-toxin is not sufficient to mediate escape from
786 phagolysosomes in upper-airway epithelial cells. *Infect Immun* **77**, 3611-3625 (2009).
787 36. M. Grosz *et al.*, Cytoplasmic replication of Staphylococcus aureus upon phagosomal escape
788 triggered by phenol-soluble modulin alpha. *Cell Microbiol* **16**, 451-465 (2014).
789 37. J. Horn, K. Stelzner, T. Rudel, M. Fraunholz, Inside job: Staphylococcus aureus host-pathogen
790 interactions. *Int J Med Microbiol* **308**, 607-624 (2018).
791 38. K. Stelzner *et al.*, Intracellular Staphylococcus aureus employs the cysteine protease
792 staphopain A to induce host cell death in epithelial cells. *PLoS Pathog* **17**, e1009874 (2021).
793 39. J. Gatfield, J. Pieters, Essential role for cholesterol in entry of mycobacteria into macrophages.
794 *Science* **288**, 1647-1650 (2000).
795 40. R. Zidovetzki, I. Levitan, Use of cyclodextrins to manipulate plasma membrane cholesterol
796 content: evidence, misconceptions and control strategies. *Biochim Biophys Acta* **1768**, 1311-
797 1324 (2007).
798 41. K. A. Joiner, S. A. Fuhrman, H. M. Miettinen, L. H. Kasper, I. Mellman, Toxoplasma gondii:
799 Fusion Competence of Parasitophorous Vacuoles in Fc Receptor-Transfected Fibroblasts.
800 *Science* **249**, 641-646 (1990).
801 42. S. Kim, M. Watarai, S.-i. Makino, T. Shirahata, Membrane sorting during swimming
802 internalization of Brucella is required for phagosome trafficking decisions. *Microbial*
803 *Pathogenesis* **33**, 225-237 (2002).
804 43. K. Stelzner *et al.*, Intracellular Staphylococcus aureus Perturbs the Host Cell Ca(2+) Homeostasis
805 To Promote Cell Death. *mBio* **11** (2020).

44. R. Y. Tsien, A non-disruptive technique for loading calcium buffers and indicators into cells. *Nature* **290**, 527-528 (1981).
45. Krones & Rühling *et al.*, Staphylococcus aureus alpha-Toxin Induces Acid Sphingomyelinase Release From a Human Endothelial Cell Line. *Front Microbiol* **12**, 694489 (2021).
46. T. Maruyama, T. Kanaji, S. Nakade, T. Kanno, K. Mikoshiba, 2APB, 2-aminoethoxydiphenyl borate, a membrane-penetrable modulator of Ins(1,4,5)P3-induced Ca2+ release. *J Biochem* **122**, 498-505 (1997).
47. T. F. Walseth, H. C. Lee, Synthesis and characterization of antagonists of cyclic-ADP-ribose-induced Ca2+ release. *Biochim Biophys Acta* **1178**, 235-242 (1993).
48. E. Naylor *et al.*, Identification of a chemical probe for NAADP by virtual screening. *Nature Chemical Biology* **5**, 220-226 (2009).
49. S. Y. Kim, B. H. Cho, U. H. Kim, CD38-mediated Ca2+ signaling contributes to angiotensin II-induced activation of hepatic stellate cells: attenuation of hepatic fibrosis by CD38 ablation. *J Biol Chem* **285**, 576-582 (2010).
50. S. Y. Rah, M. Mushtaq, T. S. Nam, S. H. Kim, U. H. Kim, Generation of cyclic ADP-ribose and nicotinic acid adenine dinucleotide phosphate by CD38 for Ca2+ signaling in interleukin-8-treated lymphokine-activated killer cells. *J Biol Chem* **285**, 21877-21887 (2010).
51. Z. L. Piedra-Quintero, Z. Wilson, P. Nava, M. Guerau-de-Arellano, CD38: An Immunomodulatory Molecule in Inflammation and Autoimmunity. *Front Immunol* **11**, 597959 (2020).
52. C. Angeletti *et al.*, SARM1 is a multi-functional NAD(P)ase with prominent base exchange activity, all regulated bymultiple physiologically relevant NAD metabolites. *iScience* **25**, 103812 (2022).
53. A. Rodriguez, P. Webster, J. Ortego, N. W. Andrews, Lysosomes behave as Ca2+-regulated exocytic vesicles in fibroblasts and epithelial cells. *J Cell Biol* **137**, 93-104 (1997).
54. J. Cerny *et al.*, The small chemical vacuolin-1 inhibits Ca(2+)-dependent lysosomal exocytosis but not cell resealing. *EMBO Rep* **5**, 883-888 (2004).
55. A. Reddy, E. V. Caler, N. W. Andrews, Plasma membrane repair is mediated by Ca(2+)-regulated exocytosis of lysosomes. *Cell* **106**, 157-169 (2001).
56. C. Tam *et al.*, Exocytosis of acid sphingomyelinase by wounded cells promotes endocytosis and plasma membrane repair. *J Cell Biol* **189**, 1027-1038 (2010).
57. A. G. Roth *et al.*, Potent and selective inhibition of acid sphingomyelinase by bisphosphonates. *Angew Chem Int Ed Engl* **48**, 7560-7563 (2009).
58. C. Muhle, J. Kornhuber, Assay to measure sphingomyelinase and ceramidase activities efficiently and safely. *J Chromatogr A* **1481**, 137-144 (2017).
59. C. Kappe, Z. H. Mohamed, E. Naser, A. Carpinteiro, C. Arenz, A Novel Visible Range FRET Probe for Monitoring Acid Sphingomyelinase Activity in Living Cells. *Chemistry* **26**, 5780-5783 (2020).
60. R. Pantůcek *et al.*, Identification of bacteriophage types and their carriage in Staphylococcus aureus. *Arch Virol* **149**, 1689-1703 (2004).
61. C. J. Ellison, W. Kukulski, K. B. Boyle, S. Munro, F. Randow, Transbilayer Movement of Sphingomyelin Precedes Catastrophic Breakage of Enterobacteria-Containing Vacuoles. *Curr Biol* **30**, 2974-2983 e2976 (2020).
62. L. C. Davis, A. J. Morgan, A. Galione, NAADP-regulated two-pore channels drive phagocytosis through endo-lysosomal Ca(2+) nanodomains, calcineurin and dynamin. *EMBO J* **39**, e104058 (2020).
63. Y. Sakurai *et al.*, Ebola virus. Two-pore channels control Ebola virus host cell entry and are drug targets for disease treatment. *Science* **347**, 995-998 (2015).
64. G. S. Gunaratne, Y. Yang, F. Li, T. F. Walseth, J. S. Marchant, NAADP-dependent Ca(2+) signaling regulates Middle East respiratory syndrome-coronavirus pseudovirus translocation through the endolysosomal system. *Cell Calcium* **75**, 30-41 (2018).
65. X. Ou *et al.*, Characterization of spike glycoprotein of SARS-CoV-2 on virus entry and its immune cross-reactivity with SARS-CoV. *Nature Communications* **11**, 1620 (2020).
66. L. C. Davis *et al.*, NAADP activates two-pore channels on T cell cytolytic granules to stimulate exocytosis and killing. *Curr Biol* **22**, 2331-2337 (2012).

859 67. A. Arredouani *et al.*, Nicotinic Acid Adenine Dinucleotide Phosphate (NAADP) and
860 Endolysosomal Two-pore Channels Modulate Membrane Excitability and Stimulus-Secretion
861 Coupling in Mouse Pancreatic β Cells. *J Biol Chem* **290**, 21376-21392 (2015).
862 68. R. S. Flannagan, R. C. Kuiack, M. J. McGavin, D. E. Heinrichs, Staphylococcus aureus Uses the
863 GraXRS Regulatory System To Sense and Adapt to the Acidified Phagolysosome in
864 Macrophages. *mBio* **9** (2018).
865 69. H. Peng *et al.*, Acid sphingomyelinase inhibition protects mice from lung edema and lethal
866 Staphylococcus aureus sepsis. *J Mol Med (Berl)* **93**, 675-689 (2015).
867 70. J. Kornhuber *et al.*, Functional Inhibitors of Acid Sphingomyelinase (FIASMAs): a novel
868 pharmacological group of drugs with broad clinical applications. *Cell Physiol Biochem* **26**, 9-20
869 (2010).
870 71. S. Kimura, T. Noda, T. Yoshimori, Dissection of the autophagosome maturation process by a
871 novel reporter protein, tandem fluorescent-tagged LC3. *Autophagy* **3**, 452-460 (2007).
872 72. M. Wiznerowicz, D. Trono, Conditional suppression of cellular genes: lentivirus vector-
873 mediated drug-inducible RNA interference. *J Virol* **77**, 8957-8961 (2003).
874 73. V. Hung *et al.*, Proteomic mapping of cytosol-facing outer mitochondrial and ER membranes in
875 living human cells by proximity biotinylation. *eLife* **6**, e24463 (2017).
876 74. F. A. Ran *et al.*, Genome engineering using the CRISPR-Cas9 system. *Nature Protocols* **8**, 2281-
877 2308 (2013).
878 75. C. J. Edgell, C. C. McDonald, J. B. Graham, Permanent cell line expressing human factor VIII-
879 related antigen established by hybridization. *Proceedings of the National Academy of Sciences*
880 **80**, 3734-3737 (1983).
881 76. S. Blättner *et al.*, Staphylococcus aureus Exploits a Non-ribosomal Cyclic Dipeptide to Modulate
882 Survival within Epithelial Cells and Phagocytes. *PLOS Pathogens* **12**, e1005857 (2016).
883 77. J. M. Vann, R. A. Proctor, Ingestion of Staphylococcus aureus by bovine endothelial cells results
884 in time- and inoculum-dependent damage to endothelial cell monolayers. *Infect Immun* **55**,
885 2155-2163 (1987).
886 78. P. D. Fey *et al.*, A genetic resource for rapid and comprehensive phenotype screening of
887 nonessential *Staphylococcus aureus* genes. *MBio* **4**, e00537-00512 (2013).
888 79. K. A. Becker *et al.*, Staphylococcus aureus Alpha-Toxin Disrupts Endothelial-Cell Tight Junctions
889 via Acid Sphingomyelinase and Ceramide. *Infect Immun* **86** (2018).
890 80. B. Giese *et al.*, Expression of δ-toxin by Staphylococcus aureus mediates escape from phago-
891 endosomes of human epithelial and endothelial cells in the presence of β-toxin. *Cell Microbiol*
892 **13**, 316-329 (2011).
893 81. J. Schindelin *et al.*, Fiji: an open-source platform for biological-image analysis. *Nat Methods* **9**,
894 676-682 (2012).

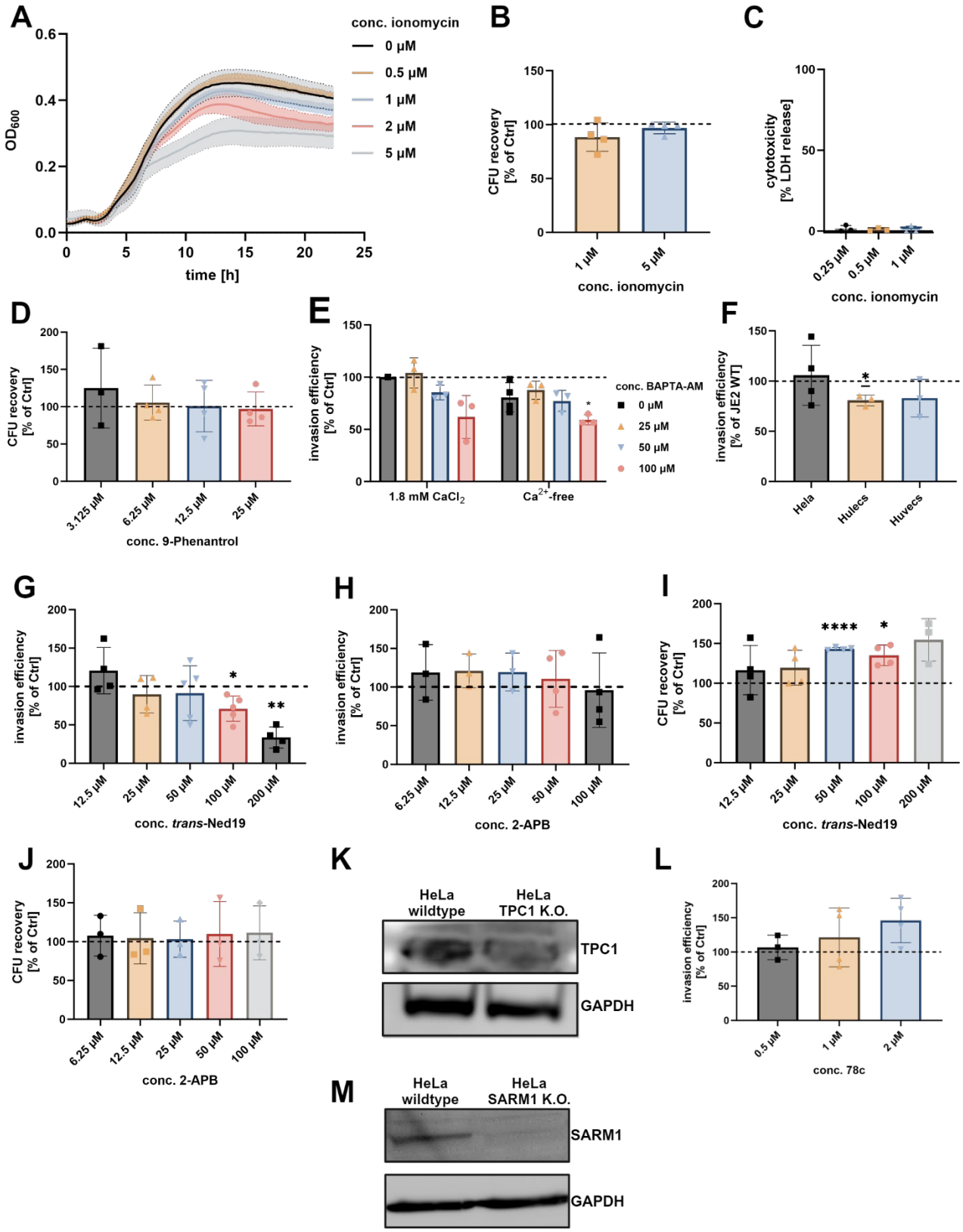

Supp. Figure 1 Supporting information for Ca^{2+}-dependent internalization of *S. aureus*.
(A) High ionomycin concentrations interfere with growth of *S. aureus* JE2. *S. aureus* JE2 was grown in in presence of varying concentrations of ionomycin. Growth (OD_{600}) was determined in a microplate reader. **(B) Ionomycin does not affect survival of *S. aureus* JE2 during infection of host cells.** HeLa cells were pretreated with varying concentrations of ionomycin and subsequently, infected with *S. aureus* JE2. After 30 min, cells were lysed and surviving extra- and intracellular bacteria were recovered by CFU count.

902 (**C) Ionomycin does not affect host cell survival.** HeLa cells were treated with the indicated concentrations
903 of ionomycin, and cytotoxicity was determined by measuring in lactate dehydrogenase (LDH) release. (**D)**
904 **9-Phenantrol does not affect survival of *S. aureus* JE2.** HeLa cells were pretreated with varying
905 concentrations of 9-Phenantrol and infected with *S. aureus* JE2. After 30 min, cells were lysed and surviving
906 extra- and intracellular bacteria were recovered by CFU plating. (**E) Chelation of intracellular but not**
907 **presence of extracellular Ca^{2+} affects *S. aureus* internalization by HeLa cells.** HeLa cells were preloaded
908 with varying concentrations of the cell-permeable Ca^{2+} chelator BAPTA-AM and then infected with *S.*
909 *aureus* JE2 in presence (+1.8 mM $CaCl_2$) or absence (Ca^{2+}-free) of Ca^{2+} in the cell culture medium. Invasion
910 efficiency was determined by CFU plating. (**F) α-toxin plays only a subordinate role during *S. aureus***
911 **uptake by host cells.** HeLa, HuLEC or HuVEC were infected with *S. aureus* JE2 wildtype or a strain
912 deficient in α-toxin production (Δ*hla*). Invasion efficiency was determined by CFU plating. The number of
913 intracellular bacteria was normalized to samples infected with the wildtype. **(G, H) *trans*-Ned19 but not 2-**
914 **APB affects invasion of *S. aureus* JE2 in HeLa.** HeLa cells were pre-treated with *trans*-Ned19 (**G**) or 2-
915 APB (**H**). 2-APB was removed from the cells shortly before infection to avoid direct contact of inhibitor
916 and bacteria (due to a bactericidal effect of 2-APB; data not shown). Then, cells were infected with *S. aureus*
917 JE2 and invasion efficiency was determined. **(I, J) *trans*-Ned19 and 2-APB have no effect on *S. aureus***
918 **JE2 in our infection protocol.** HeLa cells were pre-treated with or 2-APB (**I**) or *trans*-Ned19 (**J**). 2-APB
919 was removed from the cells shortly before infection. Then, cells were infected with *S. aureus* JE2 and, after
920 30 min, total bacteria (extra- and intracellular) were recovered by CFU plating. (**K) Reduction of TPC1**
921 **expression in a Cas9-treated cell pool (HeLa TPC1 K.O.).** TPC1 as well as GAPDH (loading control)
922 was detected in lysates of wildtype and TPC1 K.O. cells via Western blot. **(L) CD38 is not enrolled in *S.***
923 ***aureus* internalization.** HeLa cells were pretreated with the CD38 inhibitor 78c and invasion efficiency of
924 *S. aureus* JE2 was determined. (**M) Reduction of SARM1 expression in a Cas9-treated cell pool (HeLa**
925 **SARM1 K.O.).** TPC1 as well as GAPDH (loading control) was detected in lysates of wildtype and SARM1
926 K.O. cells via Western blot. Statistics: one sample t-test, Bars represent mean +/- SD. *$p \leq 0.05$, **$p \leq 0.01$,
927 ***$p \leq 0.001$, ****$p \leq 0.0001$.
928

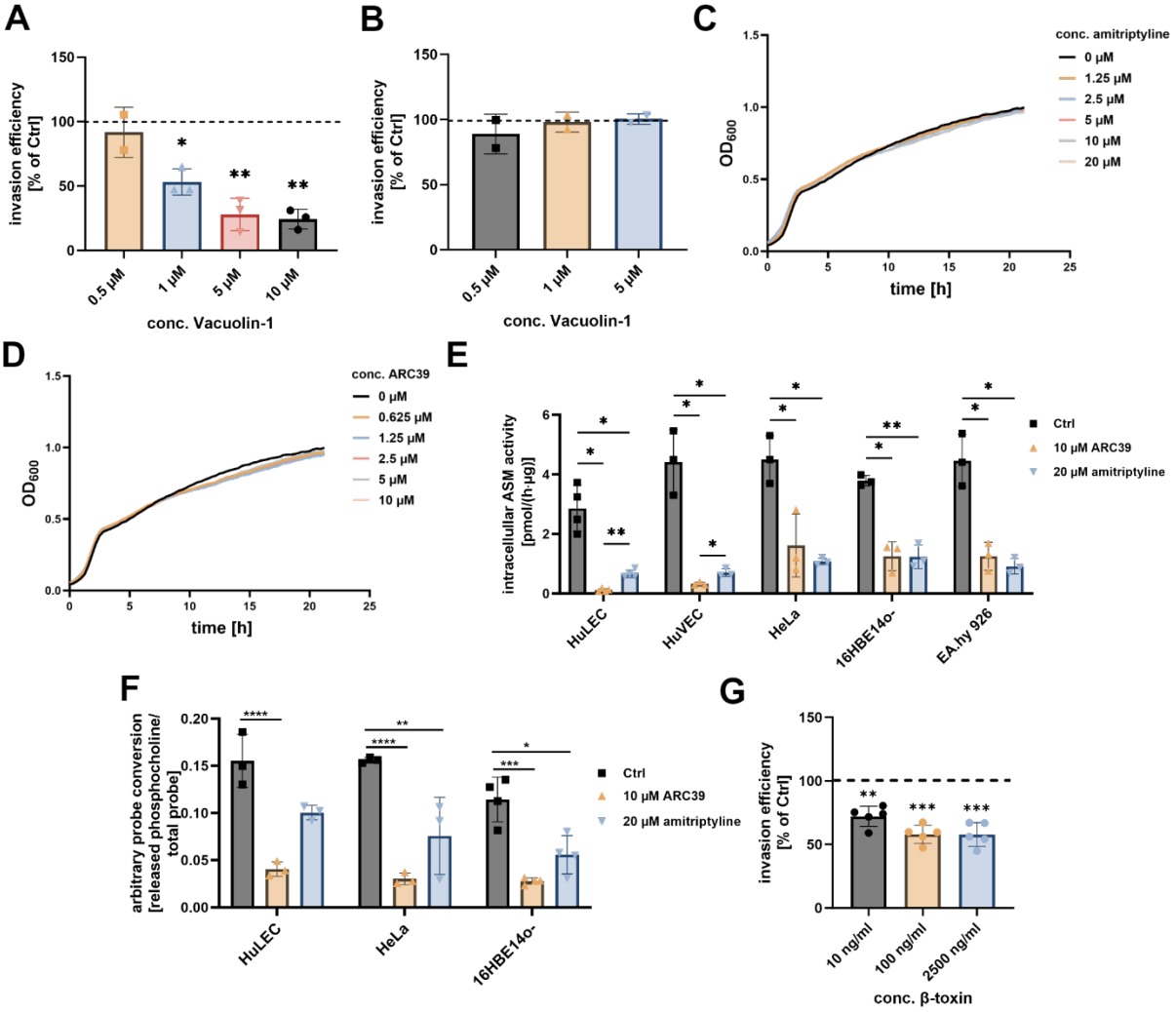

Supp. Figure 2 Supporting information for the involvement of lysosomal exocytosis and ASM in *S. aureus* invasion

(A) Blocking lysosomal exocytosis by Vacuolin-1 reduces *S. aureus* invasion in HeLa. HeLa cells were treated with increasing concentrations of the lysosomal exocytosis inhibitor Vacuolin-1. The invasion efficiency of *S. aureus* JE2 was determined 30 min p.i. **(B) Vacuolin-1 has no bactericidal effect.** HeLa cells were treated with Vacuolin-1 and infected with *S. aureus* JE2. After 30 min, total bacteria (extra- and intracellular) were recovered by CFU plating and normalized to untreated controls. **(C, D) The ASM inhibitors amitriptyline and ARC39 have no effect on growth of *S. aureus*.** *S. aureus* JE2 was grown in presence of varying concentrations of amitriptyline (**C**) or ARC39 (**D**) in BHI medium and growth was determined by measuring OD_{600} in a microplate reader. **(E, F) ASM activity and ASM inhibition by ARC39 and amitriptyline is similar among human cell lines.** Several cell lines were treated with amitriptyline or ARC39 and ASM activity within cell lysates was assessed by either thin layer chromatography-based TLC-based ASM activity assays, the conversion of BODIPY-C12-SM (**E**), or by a flow cytometry-based ASM activity assay and conversion of visible-range FRET probe (**F**). **(G) Removal of SM from the plasma membrane by β-toxin affects *S. aureus* host cell.** HeLa cells were pretreated with the indicated concentrations of β-toxin and subsequently the invasion efficiency of *S. aureus* JE2 was determined. Statistics: one sample t-test (A, G), mixed-effects model (REML) and Tukey`s multiple comparison (E, F), Bars represent mean +/- SD. *p≤0.05, **p≤0.01, ***p≤0.001, ****p≤0.0001.

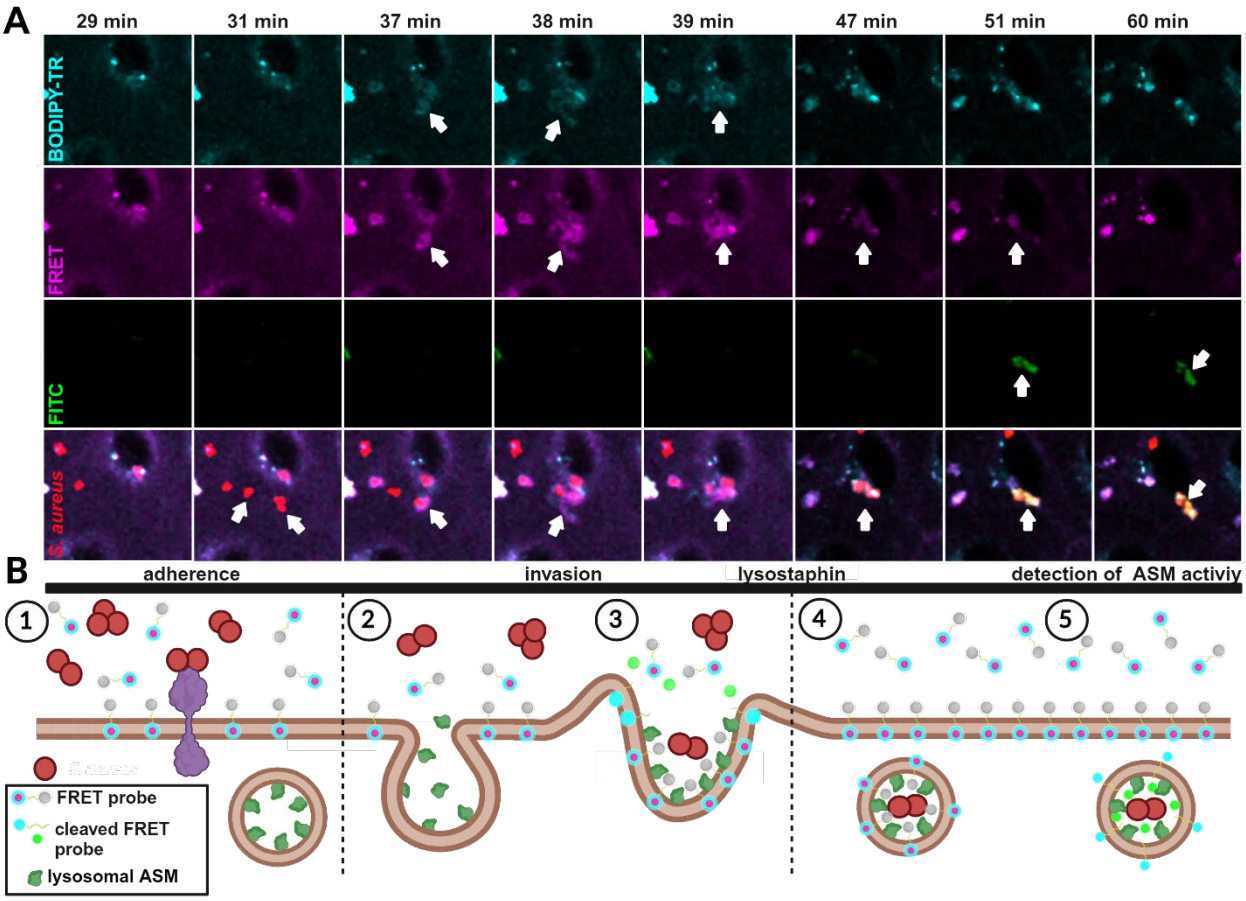

Supp. Figure 3 *S. aureus* associates with a visible-range SM probe during host cell invasion.
(A) Live cell imaging of *S. aureus* infection reveals association of the bacteria with a SM analog during cell entry. HuLEC were treated with 10 µM of a visible range FRET probe in presence of 1% FBS. Then, cells were infected with *S. aureus* JE2 in presence of the probe and infection was monitored by live cell confocal imaging. After 40 min, lysostaphin was added to remove extracellular bacteria. The BODIPY-TR signal demonstrates the localization of the probe, the FRET signal indicates an intact, non-metabolized probe, whereas FITC fluorescence indicates probe cleavage by ASM. Bacteria of interest (white arrows) adhere to host cell between 29 and 31 min p.i. **(B) Hypothetical model of *S. aureus* invasion.** (1). The interaction of bacteria with the host cell surface triggers lysosomal exocytosis, release of ASM (2) and the uptake of the bacteria (cmp. to A: at 37-39 min p.i.) by ASM-dependent membrane remodeling (3). ASM is co-internalized together with bacteria (4) and subsequently, cleaves the probe within the *S. aureus*-containing phagosome (5) (cmp: to A: increasing FITC signal starting at 47 min p.i.).

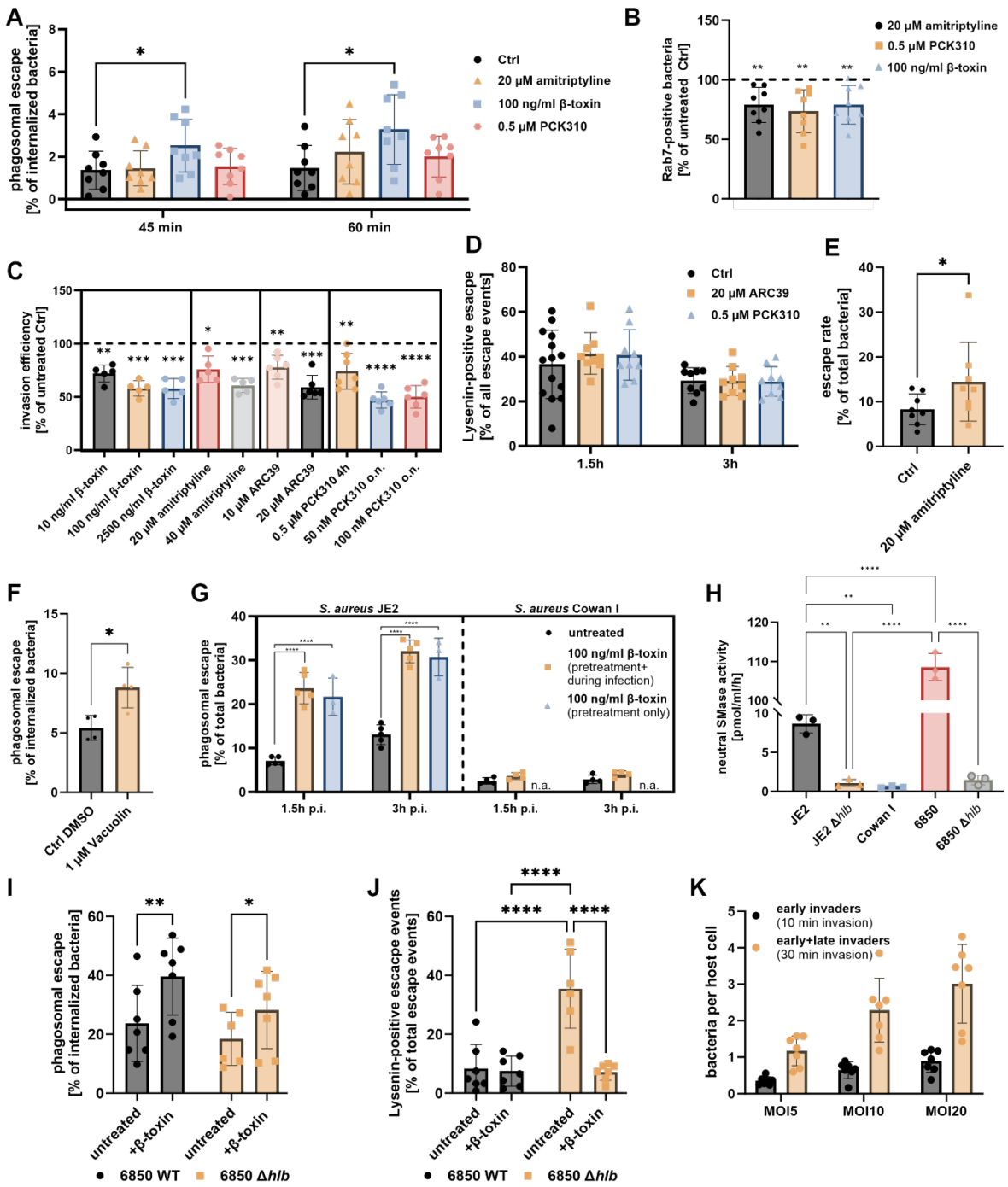

Supp. Figure 4 Supporting information for phagosomal maturation and phagosomal escape measurements.
(A) Phagosomal escape assay in early infection. A HeLa reporter cell line expressing YFP-Rab7 and RFP-CWT was treated with amitriptyline, β-toxin and PCK310 and subsequently infected with *S. aureus* JE2 for 30 min. Extracellular bacteria were removed by lysostaphin and the proportion of bacteria that acquired the phagosomal escape marker RFP-CWT was determined 45 and 60 min p.i. (n=8). **(B) Reduced association of *S. aureus* with Rab7 is not due to changes in phagosomal escape.** HeLa cells expressing YFP-Rab7 and the phagosomal escape marker RFP-CWT were treated with amitriptyline, PCK310 or β-toxin and subsequently, infected with *S. aureus* JE2 for 45 min and analyzed by CLSMs. Bacteria that escaped from phagosomes were subtracted from the data set and the proportion of residual bacteria associating with Rab7 was determined. Results of treated samples were normalized to untreated controls (n=7). **(C) β-toxin treatment and ASM inhibition reduced invasion efficiency of *S. aureus* JE2 in a dual reporter HeLa cell line.** A HeLa reporter cell line expressing RFP-CWT and Lysenin^{W20A}-YFP was treated with the indicated concentrations of β-toxin and amitriptyline for 75 min, the indicated concentrations of ARC39 for 22 h, 0.5 µM PCK310 for 4h or 50/100 nM PCK310 for 22h (o.n.) and

invasion efficiency of *S. aureus* JE2 was determined. (n≥5) **(D) Inhibition of ASM has no influence on the proportion of Lysenin^{W20A}-positive escape events.** The dual reporter cell line was infected with *S. aureus* JE2. Extracellular bacteria were removed and the proportion of bacteria that acquired the phagosomal escape marker RFP-CWT as well as the SM reporter Lysenin^{W20A}-YFP was determined by CLSM. The proportion of escaped (RFP-CWT-positive) bacteria that additionally acquired Lysenin^{W20A}-YFP was calculated. (n=9). **(E) ASM inhibition by amitriptyline increases phagosomal escape of *S. aureus* JE2.** The dual reporter cell line was infected with *S. aureus* JE2 and phagosomal escape rates were determined 3h p.i. (n=8). **(F) Blocking lysosomal exocytosis by Vacuolin-1 enhanced phagosomal escape.** HeLa RFP-CWT/Lysenin^{W20A}-YFP was pretreated with 1 µM Vacuolin-1 and infected with *S. aureus* JE2 for 10 min. Phagosomal escape rates were determined by CLSM 3 h p.i. (n=4). **(G) β-toxin pretreatment increases phagosomal escape of *S. aureus* JE2 but not *S. aureus* Cowan I.** RFP-CWT and Lysenin^{W20A} -YFP expressing HeLa were treated with 100 ng/ml β-toxin infected with *S. aureus* strains JE2 or Cowan I. Thereby, β-toxin was either removed prior to infection (pretreatment only) or was present during the whole experiment (pretreatment + during infection). By CLSM, proportions of bacteria that recruited RFP-CWT (phagosomal escape) were determined (n≥3). **(H) *S. aureus* strains vary in β-toxin expression.** The neutral SMase activity in culture supernatants of the indicated *S. aureus* strains or isogenic β-toxin mutants (Δ*hlb*) were determined by a TLC-based approach (n=3). **(I, J) β-toxin pretreatment of host cells but not β-toxin expression of endocytosed *S. aureus* affects phagosomal escape.** HeLa RFP-CWT/Lysenin^{W20A} -YFP were infected with *S. aureus* 6850 or an isogenic strain deficient in β-toxin production (Δ*hlb*). The proportion of bacteria that escaped from the phagosome as well as the percentage of phagosomal escape events that were Lysenin^{W20A} -positive were determined 3h p.i. (n=6). **(K) Increasing the MOI compensates for shorter infection times.** HeLa cells were either infected for 10 min or 30 min with varying MOIs. Then, the number of intracellular bacteria per host cell was determined 3h p.i. by CLSM. (n=7). Statistics: Mixed effects analysis (REML) with Šídák's multiple comparison (A, G), Mixed effects analysis (REML) and Tukey's multiple comparison (I, J), One-way ANOVA with Tukey's multiple comparison (H), one samples t-test (B, C), unpaired Student's t-test (E, F). Bars represent mean +/- SD. *p≤0.05, **p≤0.01, ***p≤0.001, ****p≤0.0001.

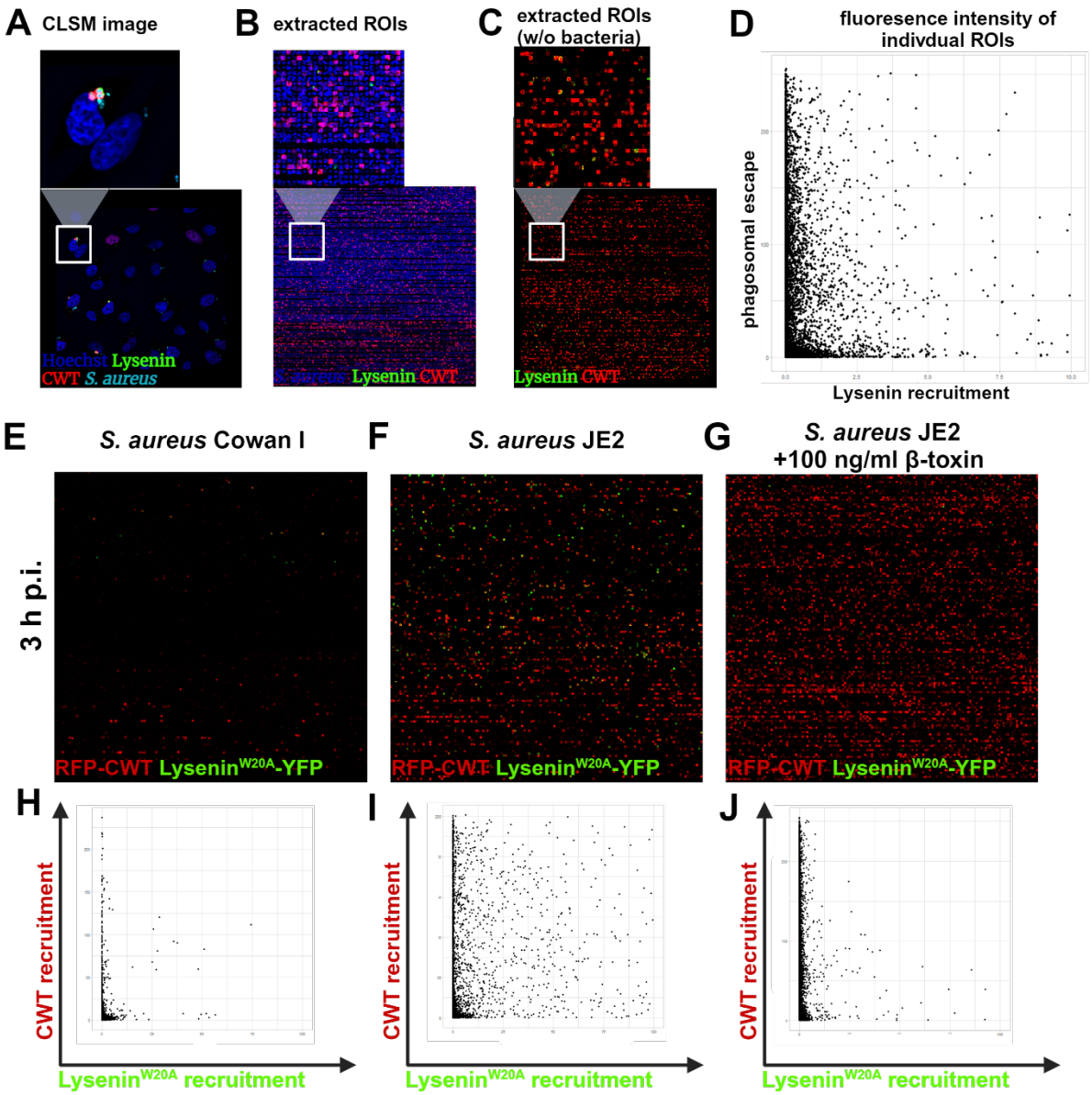

Supp. Figure 5 Evaluation of phagosomal escape and Lysenin^{W20A} recruitment during *S. aureus* infection. HeLa reporter cells expressing RFP-CWT and Lysenin^{W20A}-YFP were infected with *S. aureus* JE2, fixed and imaged by CLSM (**A**). Individual bacteria within the images were identified as regions of interest (ROIs) and extracted in each color channel. All extracted ROIs are depicted in a montage (**B**). If bacteria signals are omitted, the montage of extracted ROIs shows the proportion of reporter recruitment. The average fluorescence intensity of both reporter fluorophores is measured within each individual ROIs is plotted as dot plots (**D**). From these results, the proportion of bacteria that recruited the markers (CWT-RFP = phagosomal escape and Lysenin^{W20A} = SM-rich-phagosome) is calculated. **(E-J) Exemplary escape assay.** Montages of extracted ROIs (without bacterial fluorescence) as well as the resulting intensity measurement in individual ROIs 3 h p.i. are depicted for infections of *S. aureus* Cowan I (E, H) and JE2 (F, I) as well as an infection with *S. aureus* JE2 in which host cells were treated with 100 ng/ml β-toxin prior to infection (G, J). Data are quantified in **Figure 4**, C.

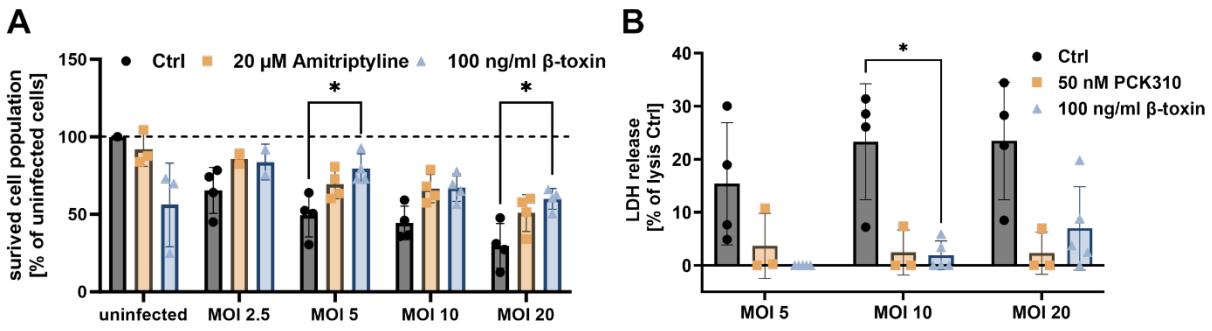

Supp. Figure 6 Inhibition of ASM and β-toxin treatment increase number of host cells remaining attached to the substratum and reduce host cell lysis during infection. HuLEC were treated with amitriptyline or β-toxin (**A**) or PCK310 and β-toxin (**B**) and were then infected with *S. aureus* JE2. After 30 min, extracellular bacteria were removed and the number of cells remaining attached to the substratum was determined (**A**) or the proportion of host cells that were lysed during the infection was measured by lactate dehydrogenase (LDH) release (**B**). Statistics: Mixed-effects analysis and Dunnett`s multiple comparison (A, B). Bars represent mean +/- SD. *p≤0.05, **p≤0.01, ***p≤0.001, ****p≤0.0001.

Supplementary Videos

Supp. Video 1 *S. aureus* associates with BODIPy-FL-C_{12}-sphingomyelin during invasion
(for further details, see Figure 3, a)

Supp. Video 2 *S. aureus* associates with a visible-range FRET probe during invasion
(for further details, see Supp. Figure 3)

Supp. Video 3 β-toxin pretreatment protects HuLEC from *S. aureus* infection
(for further details see Figure 5, c)